Akademie věd České republiky

Teze disertace k získání vědeckého titulu "doktor věd"
ve skupině chemických věd

Singlet oxygen producing sensitizers: from molecular photophysics to photofunctional materials

Komise pro obhajoby doktorských disertací v oboru Anorganická chemie

Kamil Lang

Ústav anorganické chemie AVČR, v.v.i.

Řež, 2014

Contents

Résumé

This thesis reviews my research on the photophysical and photochemical properties of porphyrin sensitizers confined in water-soluble host-guest complexes or in host matrices including layered hydroxides and polymers. The properties of photoactive porphyrins constrained within hosts are altered and cannot be directly extrapolated from the known behavior of their individual components. The sensitizers studied were mostly of the porphyrin type; however, two other groups of novel sensitizers, hexanuclear molybdenum clusters and boron clusters, were also investigated. Particular attention was paid to the sensitizers producing singlet oxygen by energy transfer from their excited triplet states to molecular oxygen. Because the kinetic parameters of the triplet states predetermine the formation of singlet oxygen, the excited-state dynamics of the sensitizers were characterized by steady-state and time-resolved spectroscopy techniques.

The development of a new class of photofunctional hybrid materials was based on porphyrin sensitizers intercalated in layered metal hydroxides. The metal hydroxide layers of layered hydroxides can be viewed as spacers separating compartments containing the porphyrin molecules, whose arrangement imposes specific structural, thermal, chemical, and photochemical properties on the materials. Investigation of the embedded porphyrin sensitizers in polymeric nanofiber materials and layered hydroxide/polymer composites, in which layered hydroxides serve as nanofillers and nanocontainers of photoactive porphyrins, allowed for the fabrication of eco-friendly and gas permeable polymers with bactericidal and virucidal surfaces that are activated by visible light. We also prepared and characterized the first metal-organic frameworks with singlet oxygen-sensitizing ability. Our research on layered metal hydroxides led to the development of new methods of hydroxide delamination and to the use of hydroxide nanosheets for the preparation of functional films (for luminescent, photocatalytic, and electrochemical activity) with an adjustable thickness.

The unifying theme of the research was to utilize the photophysical and photochemical properties of the embedded sensitizers for the development of materials whose function is triggered by visible light, i.e., materials with bactericidal surfaces or materials acting as solid sensitizers or oxygen sensors.

Abbreviations

CD	Cyclodextrin
clx*m*	*p*-Sulfonatocalix[m]arene (*m* = 4,6,8)
DS	Dodecyl sulfate
LDHs	Layered double hydroxides
LZHs	Layered zinc hydroxide salts
MOF	Metal-organic framework
Mg_RAl-LDH-PdTPPC	Layered double hydroxide with a Mg/Al molar ratio *R* and intercalated with PdTPPC (and analogously for other LDHs)
LZH-TPPS	Layered zinc hydroxide intercalated with TPPS
LREHs	Layered rare-earth hydroxides
LEuH-PdTPPS	Layered europium hydroxide intercalated with PdTPPS
MTPPC, MTPPS, MTPP	Metal complexes of TPPC, TPPS, or TPP
PDT	Photodynamic therapy
PU	Polyurethane
SBU	Secondary building unit
SODF	Singlet oxygen-sensitized delayed fluorescence
TPP	5,10,15,20-Tetraphenylporphyrin
TPPS	5,10,15,20-Tetrakis(4-sulfonatophenyl)porphyrin
TPPC	5,10,15,20-Tetrakis(4-phosphonatophenyl)porphyrin
TMPyP*n*	5,10,15,20-Tetrakis(*N*-methylpyridinium-*n*-yl)porphyrin
XRD	X-ray diffraction
ZnPc	Zinc phthalocyanine

Symbols

Φ_f , Φ_p, Φ_T	Quantum yields of fluorescence, phosphorescence, or triplet states
Φ_Δ	Quantum yield of singlet oxygen formation

1. Foreword

Photosensitized production of singlet oxygen from molecular oxygen has found far-reaching applications in chemistry and biology. The reaction is based on the excitation of a sensitizer molecule by light, followed by energy transfer to the ground triplet state oxygen which, in turn, is excited to its singlet state. Singlet oxygen, a highly reactive species, is involved in numerous oxidative processes and can cause serious damage to biological materials. The oxidative potential of singlet oxygen can also be exploited for use in chemical syntheses, for the photodynamic treatment of cancer, and for antimicrobial photodynamic therapy. Singlet oxygen reactions have become an interdisciplinary topic that spans photophysics, quantum chemistry, photochemistry, photobiology, and photomedicine.[1,2,3]

The observed poor correlation between photophysical parameters of sensitizers and their photosensitizing efficacy in a complex environment turned my attention to the interactions of sensitizers with surrounding entities. Understanding these interactions could help explain the unexpected differences in sensitizer photophysical and photochemical properties. In chemical terms, the noncovalent interactions of sensitizers with the microenvironment may play a key role in controlling the sensitizer properties. The research progressed along two parallel courses:

1. *Noncovalent interactions of sensitizers and their photophysical and photochemical properties*. Noncovalent binding of porphyrin sensitizers to biopolymers (proteins, nucleic acids) and host molecules, such as cyclodextrins and calixarenes, does not restrict the formation of excited states, but it influences their yields and the kinetics of their reactions.[4] Evidently, careful assessment of the binding effects on the molecular level is a rational way to understand photosensitized processes in complex environments. We also investigated nanostructured and polymeric host matrices with embedded porphyrins to reduce their undesired aggregation and to eliminate a "hostile" environment that can affect the porphyrin sensitizing activity.
2. *Photofunctional materials*. We investigated hybrid materials based on porphyrins intercalated in layered metal hydroxides [A1]. Layered hydroxides were found to act as hosts that keep the photoactive molecules organized in a two-dimensional expandable interlayer space and separated from the surroundings. Such hybrids are not only easy to use as transport materials; they also turn out to be suitable for the fabrication of light-triggered materials with bactericidal functionality. Polymeric nanofiber materials doped with porphyrins have bactericidal and virucidal surfaces

upon visible light irradiation. Molybdenum cluster complexes were found to be promising molecules for the preparation of luminescent materials and oxygen sensors.

2. Photosensitized reactions of molecular oxygen

Oxygen molecules, having absorption in the vacuum UV region, can be hardly excited by direct exposure to common sources of UV/Vis radiation. The indirect path of oxygen excitation, the photosensitized reaction, is therefore the main pathway involving excited forms of oxygen. Photosensitized oxygen reactions are classified as Type I and Type II according to the nature of the quencher.[5] Quenching of the excited sensitizer by molecular oxygen proceeds as energy transfer, yielding singlet oxygen, or as electron transfer, yielding the superoxide radical anion O_2^- (Type II reactions).

Sensitization. A photosensitized reaction involves the excitation of a sensitizer into higher electronic states by light. Processes occurring after excitation can be summarized as follows: excited singlet states, $^1P^*$, decay to ground states, ^1P, by fluorescence (Eq. 1) and vibrational relaxation. Intersystem crossing leads to triplet states, ^3P, (Eq. 2) that are deactivated spontaneously *via* vibrational relaxation, phosphorescence emission (Eq. 3), or by interaction with oxygen to form $O_2(^1\Delta_g)$ and $O_2(^1\Sigma_g^+)$ (Eq. 4). The higher excited state, $O_2(^1\Sigma_g^+)$, has a very short lifetime; hence, the relatively long-lived $O_2(^1\Delta_g)$, referred to as "singlet oxygen", is generally accepted as a decisive species involved in photosensitized reactions (Figure 1). The excited singlet states of most sensitizers are too short-lived to be effectively quenched by oxygen to form singlet oxygen. Detailed discussion of all of these processes can be found elsewhere.[3,4]

$$^1P^* \longrightarrow {}^1P + h\nu_f \quad (1)$$

$$^1P^* \longrightarrow {}^3P \quad (2)$$

$$^3P \longrightarrow {}^1P + h\nu_p \quad (3)$$

$$^3P + O_2(^3\Sigma_g^-) \longrightarrow {}^1P + O_2(^1\Delta_g) \quad (4)$$

$$O_2(^1\Delta_g) \longrightarrow O_2(^3\Sigma_g^-) + h\nu_p \quad (5)$$

Sensitizers. Numerous dyes and complexes produce singlet oxygen and are considered suitable for photodynamic therapy (PDT); nevertheless, the majority of the sensitizers investigated in this context have a porphyrinic structure. The reasons for this preference are the extensive knowledge of porphyrin chemistry and their inherent similarity to natural porphyrins in living matter. For photodynamic applications, the sensitizers should possess

certain characteristics, such as absorption and emission in the red spectral region to minimize interference with the living tissue, high quantum yield of singlet oxygen formation (Φ_Δ), low toxicity, and good chemical and photochemical stability.

My research is focused on porphyrins and related macrocycles in solutions[4] and solid materials [A1] (Sections 3 and 5), hexanuclear molybdenum cluster complexes as relevant alternatives to the sensitizers so far used (Section 4.1), and boron clusters (Section 4.2.).

Figure 1. Transitions between electronic states of oxygen (*ic* - internal conversion, *isc* - intersystem crossing, *f* - fluorescence, *p* - phosphorescence).

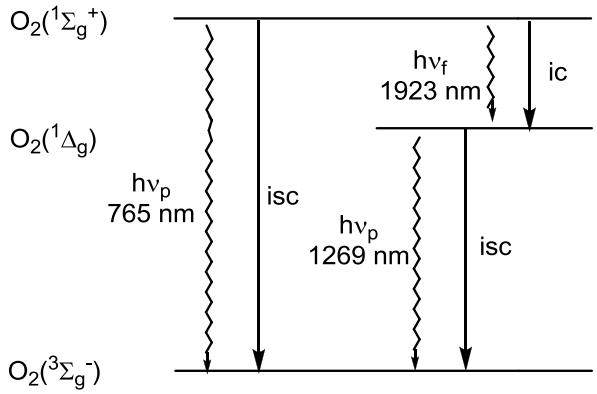

Experimental methods. The photophysical results presented in this work were obtained by steady-state and time-resolved spectroscopy techniques with a time resolution ranging from picoseconds to seconds (luminescence, transient absorption, and diffuse reflectance transient absorption). The formation of $O_2(^1\Delta_g)$ is indicated by oxygen quenching of the sensitizer triplet states (Eq. 4). However, direct evidence of $O_2(^1\Delta_g)$ formation and its consecutive reactions was provided by measuring $O_2(^1\Delta_g)$ luminescence at approximately 1270 nm in steady-state or time-resolved regimes (Eq. 5) (e.g., Figure 13).

3. Porphyrinic sensitizers

Porphyrins and related macrocycles are well known sensitizers with rich fluorescence properties and reactive triplet states. We were especially concerned with sensitizer spectral and photophysical properties and the changes induced by noncovalent binding with biopolymers, synthetic carriers (Section 3.1.), anionic and cationic species.[4,6] The molecular structures of the sensitizers considered in this work are presented in Figure 2.

Figure 2. Molecular structures of (a) porphyrins and (b) phthalocyanines. Abbreviations used throughout the text: 5,10,15,20-tetraphenyl porphyrin (TPP) (R = H, M = H_2), 5,10,15,20-tetrakis(4-sulfonatophenyl) porphyrin (TPPS) (R = SO_3^-, M = H_2); 5,10,15,20-tetrakis-(carboxyphenyl)porphyrins (TPPC) (R = COO^-, M = H_2); zinc phthalocyanine (ZnPc).

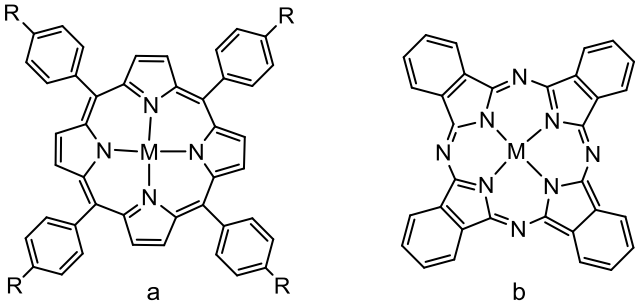

In general, porphyrinic molecules tend to form closely stacked assemblies (aggregates) in which the absorbed energy dissipates through competitive decay channels.[4] In our comprehensive study on the aggregation properties of meso-tetratolylporphyrins bearing cationic substituents, we specified how the formation of respective aggregates can be affected by porphyrin substitution, ionic strength, and temperature of solution [A2]. The aggregation was accompanied by considerable changes of absorption spectra, and the positions of aggregate absorption bands could be successfully predicted by using the exciton point-dipole model. Achiral cationic porphyrins can spontaneously aggregate to form highly ordered chiral assemblies that are structurally related to the arrangement of achiral cationic porphyrins on helical DNA backbones [A3]. The chirality was controlled by the type of anionic counterpart.

The aggregation causes a significant quenching of excited states, including triplet states and the subsequent formation of $O_2(^1\Delta_g)$. Because of this, aggregation was an undesirable process in our studies. One way to prevent aggregation was to immobilize individual sensitizer molecules in inorganic hosts of ordered structures such as layered metal hydroxides[7] or layered silicates.[8] We performed these studies with anionic porphyrins (sulfonate and carboxyl substituents) [A1] and with cationic porphyrins (mostly *N*-methyl pyridinium substituents). Our results on layered metal hydroxide hybrids are described in Section 5.1. This approach produces materials with defined microscopic structure, specific sensitizer alignment, host variability, and the increased stability of the photoactive molecules. The effects on sensitizer properties can be attributed to noncovalent interactions with the layers surrounding the intercalated molecules and ions.[9]

The embedding of water-insoluble sensitizers in polymeric nanofiber materials allows for the preparation of new photobactericidal and photovirucidal surfaces. These functionalities

are based on the combination of the photosensitizing activity of porphyrins with the high surface area, flexibility, lightness, and good light and oxygen penetrability of nanofibers (Section 5.2.).

3.1. Noncovalently bound porphyrin sensitizers in solutions

The common feature of noncovalent interactions is a bond energy distinctly lower than the energy of covalent bonding. Typical ΔH values of a simple covalent bond range from 150 to 500 kJ mol^{-1}, whereas the ΔH values of noncovalent interactions are below 150 kJ mol^{-1}, with the weakest being on the order of a few kJ mol^{-1}.[10]

Knowledge of the photophysical properties of sensitizers is essential for the assessment of the reactivity of electronically excited states with target molecules (Type I reactions) or with molecular oxygen (Type II reactions). The best sensitizing effect can be attained with a monomeric porphyrinic sensitizer that is closely associated with a target molecule. Hence, we investigated the binding constants, spectral properties, triplet lifetimes, and quantum yields Φ_T and Φ_Δ.

3.1.1. Calixarenes

Calix[n]arenes are macrocyclic oligophenols with a cyclic framework linked by methylene bridges. Water-soluble *p*-sulfonatocalix[*m*]arenes (Figure 3) possess three-dimensional, flexible, π electron-rich cavities that can adopt different conformations, can form complexes with a variety of compounds, and can be used in biomedical applications.[11]

The interactions of TMPyP*n* with sulfonated calixarenes were examined in three consecutive reports. First, we investigated the binding of TMPyP4 to a series of *p*-sulfonatocalix[m]arenes (clx*m*, *m* = 4,6,8) and studied the photophysical properties of TMPyP4/clx*m* complexes (Table 1) [A4]. Calixarene clx4 exhibited a high binding affinity toward TMPyP4 to form a 1:1 complex, whereas clx6 and clx8 bound up to two molecules of TMPyP4. In all cases, electrostatic attraction was the dominant binding mode. The binding led to considerable decreases in the quantum yields of the triplet and excited singlet states and to the shortening of the singlet and triplet lifetimes of TMPyP4. The quenching mechanism was, for the first time, elucidated as electron transfer between calixarene phenolates and the excited states of TMPyP4.

In the next paper, we extended our research to isoelectronic TMPyP2 and 5,10,15,20-tetrakis(4-trimethylammoniophenyl)porphyrin (TMAPP) and to their interactions with clx4,

thiacalix[4]arene-*p*-tetrasulfonate, and sulfonylcalix[4]arene-*p*-tetrasulfonate [A5]. We observed the quenching of the excited states of TMPyP2. In the case of TMAPP, the binding led to extended porphyrin aggregation.

Figure 3. Structure of porphyrins (TMPyP*n*) and *p*-sulfonatocalix[*m*]arenes (clx*m*). Abbreviations used: 5,10,15,20-tetrakis(*N*-methylpyridinium-*n*-yl)porphyrin (TMPyP*n*).

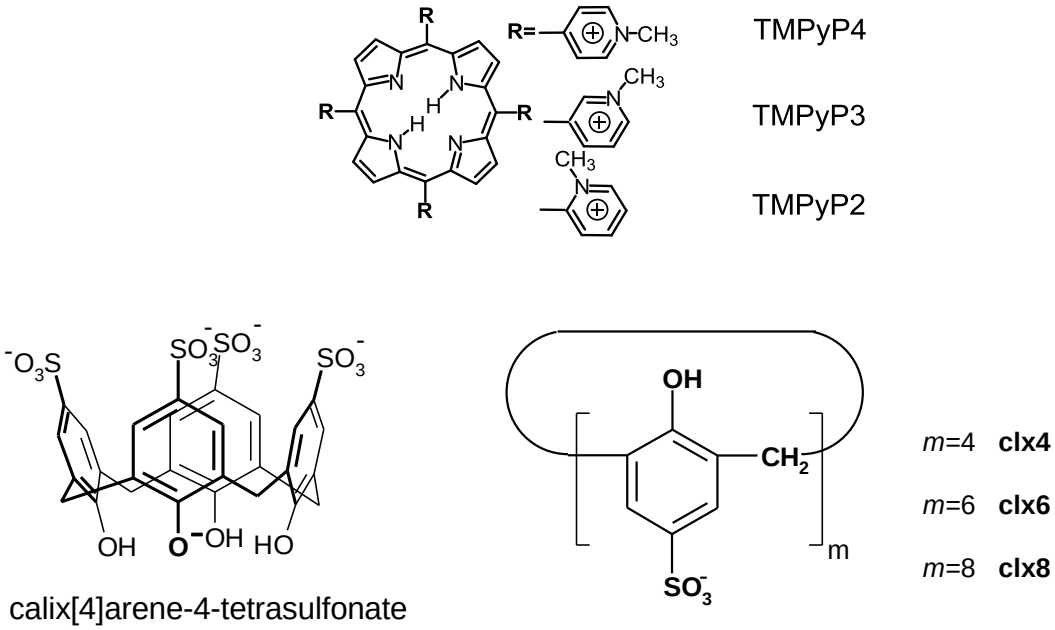

Table 1. Photophysical characteristics of TMPyP4 bound to *p*-sulfonatocalix[m]arenes:
Φ_f is the fluorescence quantum yield, τ_T is the triplet lifetime in deoxygenated solutions, τ is the triplet lifetime in air-saturated solutions, k_q is the bimolecular rate constant for the quenching of the triplet states by oxygen, and Φ_T is the quantum yield of the triplet states. For the characteristics of TMPyP4 see Table 2.

Host	Φ_f	τ_T/μs	τ/μs	k_q/M^{-1}s^{-1}	Φ_T
clx4	0.031	75	2.4	1.5×10^9	0.57
clx6	0.008	16	2.2	1.6×10^9	0.18
clx8	0.001	31	2.6	1.4×10^9	0.03

Because the nanosecond time resolution of fluorescence experiments performed in the previous study [A5] was not sufficient to describe the dynamics of TMPyP*n* excited states, the studies were complemented by femtosecond transient absorption measurements of TMPyP*n*–clx*m* complexes in conjunction with DFT calculations [A6]. It was found that the quenching of the excited singlet states of the complexes depends on the number of ionized phenolic

groups of clx*m* and can be correlated with the partial electron density transfer from O^- to peripheral methylpyridinium substituents rather than to the porphyrin ring.

The key conclusions are as follows:

- The ultrafast excited-state dynamics of TMPyP*n* are related to the redistribution of electron density within the complexes. The electronic density redistribution decreases in the order TMPyP4 > TMPyP3 > TMPyP2, and the same order is observed for the increase in the fluorescence lifetimes.
- In the case of TMPyP*n*–clx*m* complexes, partial intramolecular charge separation proceeds predominantly from the ionized O^- groups of clx*m* to the methylpyridinium peripheral substituents of TMPyP*n*. The electron density redistribution within the TMPyP4–clx*m* (m = 4, 6) complexes in the ground and excited S_1 states increases with the number of O^- groups in clx*m* and can be linked to the increase of quenching efficiency of the S_1 states. The quenching of the S_1 states of TMPyP*n*–clx*m* (n = 2 and 3) can be described similarly as in the TMPyP4 complexes, *i.e.*, by the electron density transfer to methylpyridinium substituents.
- Differences in the excited-state dynamics of the complexes of TMPyP*n* positional isomers with clx*m* are related to the steric and electron-accepting effects of *N*-methylpyridinium substituents. The most effective quenching in the series of clx8 complexes is observed for TMPyP2.
- Clx4 is a potential carrier for cationic porphyrins because a moderate influence on the excited states is compensated by the high solubility and stability of the complexes.

3.1.2. Cyclodextrins

The most common cyclodextrins (CDs) consist of 6, 7, or 8 α-1,4-D-glucopyranose units arranged in a truncated cone and denoted as α-CD, β-CD or γ-CD, respectively (Figure 4).[12] The interior, lined with C–H groups and glycosidic oxygen bridges, is hydrophobic in comparison with the exterior, which is hydrophilic due to the presence of hydroxyl groups. Consequently, CDs are water-soluble and form inclusion host–guest complexes with a variety of molecules. Cyclodextrins are frequently used to improve the resistance of pharmaceuticals to thermal and oxidative degradation, to limit side effects, to increase solubility, and to prevent aggregation.[13] We were concerned with the carrier function of CDs for porphyrin sensitizers.

The binding stoichiometries of water-soluble TPPS, TPPC, and TMPyP4, and some of

their metallocomplexes (Eqs. 6 and 7), binding constants, and photophysical properties were described in several communications [A4,A7,A8].[14]

$$\text{Sens} + \text{CD} \rightleftharpoons \text{Sens-CD} \quad (6)$$

$$\text{Sens-CD} + \text{CD} \rightleftharpoons \text{Sens-(CD)}_2 \quad (7)$$

The binding influenced the molecular form of the sensitizers: (i) porphyrin aggregates were monomerized because the driving force of the complex formation exceeded the energy gain from the stacking of the porphyrin units; (ii) protonation of TPPS pyrrole nitrogen atoms was reduced. The higher the binding constant was, the more pronounced porphyrin monomerization was.

Figure 4. Schematic representation of CDs.

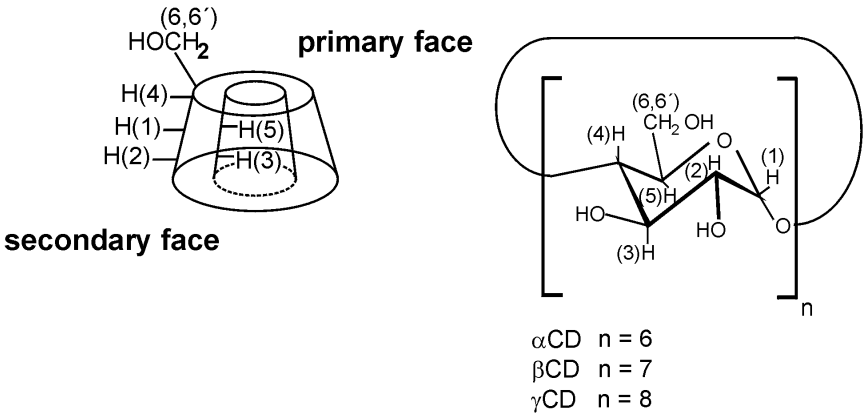

Tetraphenylporphyrin sensitizers, TPPS, ZnTPPS, PdTPPS, and TPPC4, formed 1:1 (Eq. 6) and 1:2 (Eq. 7) complexes with native or 2-hydroxypropylated CDs (hpCDs) in neutral aqueous solutions. The inclusion of the sensitizers in CDs led to bathochromic shifts of the porphyrin Soret bands, as well as prolongation of the triplet states lifetimes and slower quenching of the triplet states by oxygen (Table 2). The triplet lifetime extension can be attributed to a combined effect of the exclusion of water molecules from the solvation shell of porphyrins and the reduction of collisional quenching by solvent molecules. The photophysical parameters Φ_f, Φ_T, and Φ_Δ remained unchanged. In contrast, the native CDs did not affect the behavior of the TMPyP triplet states.

According to NMR experiments, we classified the binding modes into three categories [A8]:[4]

1. *Inclusion of meso-phenyl substituents through the secondary face* is a typical mode for β-CD and functionalized β-CDs.
2. *Inclusion of meso-phenyl substituents through the primary face* is a typical mode for γ-

CDs. The size of the secondary face is larger than that of β-CDs and, therefore, the inclusion of the *meso*-phenyl substituent from the primary face is more favorable.

3. *Non-specific external binding* was, for the first time, described for cationic TMPyP4 with native, per-methylated, sulfonated, and dimethyl-sulfonated CDs [A8]. The high affinity of TMPyP4 toward sulfonated CDs was due to ion pairing between the *N*-methylpyridinium-4-yl peripheral substituents of TMPyP and the sulfonate groups.

We found that anionic tetraphenylporphyrins bound with CDs remain good sensitizers and are protected against the influence of the environment. Thus, CDs are suitable carriers of the porphyrin sensitizers.

Table 2. Photophysical characteristics of some porphyrins bound to CDs in aqueous solution: Φ_Δ is the quantum yield of singlet oxygen formation, and other symbols are the same as in Table 1.

Complex	Φ_f	τ_T/μs	τ/μs	k_q/M^{-1}s^{-1}	Φ_T	Φ_Δ
TPPS	0.06[a]	290	2.0	1.8×10^9	0.76[b], 0.79[b]	0.62[c]
TPPS/hpα-CD	-	290	2.2	1.6×10^9	-	-
TPPS/hpβ-CD	0.05	2000	11.9	3.0×10^8	0.76	0.60
TPPS/hpγ-CD	-	2100	3.6	1.0×10^9	-	-
TMPyP4	0.046[d]	160	1.8	2.0×10^9	0.89[d]	-
TMPyP4/hpβ-CD	0.058	640	1.9	1.9×10^9	1.00	-

[a] T. Gensch, S. E. Braslavsky, *J. Phys. Chem. B* 101 (1997) 101-108. [b] R. Bonnet, R. J. Ridge, E. J. Land, R. S. Sinclair, D. Tait, T. G. Truscott, *J. Chem. Soc., Faraday Trans. I* 78 (1982) 127-136; J. Davila, A. Harriman, *Photochem. Photobiol*. 51 (1990) 9-19. [c] F. Wilkinson, W. P. Helman, A. B. Ross, *J. Phys. Chem. Ref. Data* 22 (1993) 113-262. [d] K. Kalyanasundaram, *Inorg. Chem*. 23 (1984) 2453-2459; V. S. Chirvony, V. A. Galievsky, N. N. Kruk, B. M. Dzhagarov, P.-Y. Turpin, *J. Photochem. Photobiol. B: Biol*. 40 (1997) 154-162.

4. Novel sensitizers

4.1. Hexanuclear molybdenum cluster complexes

Metal complexes with long-lived triplet states and luminescence have attracted a considerable interest over the past few years for their prospective applications as are light-emitting devices, dye-sensitized solar cells, optical oxygen sensors, and sensitizers. These complexes usually contain metals like Ir, Pt, Ru, or Os that are expensive and highly toxic. We suppose that hexanuclear molybdenum cluster complexes represent a relevant alternative.

The cluster core is a nanometer-sized octahedron of Mo^{2+} atoms linked together by metal-metal bonds and associated with eight strongly bonded inner ligands (X) and six labile apical ligands (Y) to form a $[Mo_6X_8Y_6]^{2-}$ cluster unit (Figure 6). The deliberate choice of apical organic or inorganic ligands allows for tuning cluster properties - solubility, charge, stability, and photophysical parameters. Of all the cluster complexes, $[Mo_6Cl_{14}]^{2-}$ has been the most extensively studied so far. It has intensive phosphorescence in the range of 600-900 nm associated with high Φ_L and Φ_Δ values; however, weak absorption in the visible region is unfavorable for a number of applications in light harvesting.[15,16] We suggested that the so far much less explored complexes with the $\{Mo_6I_8\}$ cluster core[17] may overcome this problem.

Figure 6. Schematic structure of the complexes (blue: molybdenum, olive: ligands).

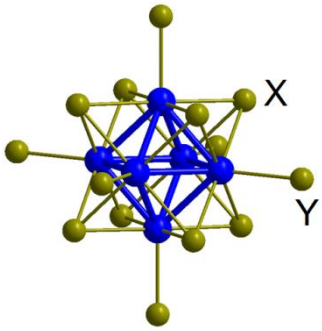

We investigated the synthetic procedures, excited-state dynamics, phosphorescence, and redox properties of a series of $(n\text{Bu}_4\text{N})_2[Mo_6X_{14}]$ and $(n\text{Bu}_4\text{N})_2[Mo_6X_8(CF_3COO)_6]$ (X = Cl, Br, or I) (Table 3) [A9,A10]. As well, we presented the crystal structures of new complexes $(n\text{Bu}_4\text{N})_2[Mo_6I_8(CF_3COO)_6]$ [A10] and $(n\text{Bu}_4\text{N})_2[Mo_6Br_8(CF_3COO)_6]$ [A9]. Our study established a considerable effect of the apical ligands on the photophysical and redox properties in solution. The increase of the mass of the inner halogen ligands decreased the corresponding oxidation potentials. The presence of the apical trifluoroacetate ligands, CF_3COO^-, significantly augmented the oxidation potential. Except for $[Mo_6Cl_8(CF_3COO)_6]^{2-}$, all the complexes displayed strong red phosphorescence in acetonitrile and no photobleaching. For the halide series, the Φ_p values and the emission maxima were only slightly affected by the nature of the halogen. However, placing the CF_3COO^- ligands in the apical positions induced a significant blue shift of the emission bands and dramatically increased the phosphorescence efficiency. Indeed, $[Mo_6I_8(CF_3COO)_6]^{2-}$ exhibited the value of Φ_p as high as 1, that is to the best of our knowledge the highest value reported for hexanuclear clusters (M = Mo, Re, W) so far [A10].

Time-resolved transient absorption measurements showed that the intersystem crossing

from the excited singlet states was ultrafast with time constants between < 120 fs and 1.68 ps and led to hot triplet states. The cooling of the hot triplet states, not observed only for $[Mo_6I_8(CF_3COO)_6]^{2-}$, occurred at a ps time scale and was attributed to electronic redistribution over the triplet state sublevels. The formation of $O_2(^1\Delta_g)$, suggested earlier indirectly on the basis of photooxidation experiments for some complexes,[16] was revised by direct measurements of $O_2(^1\Delta_g)$. The high Φ_Δ values reflect the efficiency of the intersystem crossing.

Table 3. Photophysical properties of cluster complexes in acetonitrile at room temperature: λ_p is the maximum of the luminescence emission band, Φ_p is the quantum yield of phosphorescence in oxygen-free acetonitrile, τ_T is the lifetime of the triplet states in argon-saturated acetonitrile, k_q is the bimolecular rate constant for the quenching of the triplet states by oxygen, and Φ_Δ is the quantum yield of $O_2(^1\Delta_g)$ formation in oxygen-saturated acetonitrile.

Compound	λ_p/nm	Φ_p	τ_T/μs	k_q/$M^{-1}s^{-1}$	Φ_Δ
$[Mo_6Cl_{14}]^{2-}$	744	0.15	180	3.2×10^7	0.92
$[Mo_6Br_{14}]^{2-}$	757	0.13	135	5.1×10^7	0.87
$[Mo_6I_{14}]^{2-}$	730	0.12	90	2.2×10^8	0.63
$[Mo_6Cl_8(CF_3COO)_6]^{2-}$	672, 725	0.008	290	-	<0.05
$[Mo_6Br_8(CF_3COO)_6]^{2-}$	708	0.30	335	7.4×10^7	0.86
$[Mo_6I_8(CF_3COO)_6]^{2-}$	673	1.0	270	2.3×10^8	0.85

Our results showed that varying of the apical ligands allows for tuning of cluster redox and optical properties. Our discovery that $[Mo_6I_8(CF_3COO)_6]^{2-}$ has Φ_p and Φ_Δ values of 1 and 0.85, respectively, made the preparation of cluster-based photofunctional materials possible (Section 5.2.). We assume that the coordination of ligands to the $\{Mo_6I_8\}$ cluster core *via* carboxylic functions is a promising approach for obtaining hybrid cluster complexes with designed properties.

4.2. Boron hydride clusters

Our interest in boron hydride clusters was initiated by the paper of Pitochelli and Hawthorne, who described the syntheses of *anti*- and *syn*-isomers of octadecaborane(22) (denoted here as *anti*-$B_{18}H_{22}$ and *syn*-$B_{18}H_{22}$, Figure 7). They stated that the hydrocarbon solutions of *anti*-$B_{18}H_{22}$ exhibit purple fluorescence.[18] No emission characteristics were provided. Since then, one Russian group has reported on the luminescence of some solid

borane and carborane clusters.[19] In fact, the photophysics of boron hydride clusters is practically unknown. In light of the growing interest in the applications of boron clusters in biology and medicine, we pursued the detailed structural, spectral, and photophysical characterization of $B_{18}H_{22}$ skeletons [A11,A12].

Figure 7. Molecular structures of (A) *syn*-$B_{18}H_{22}$ and (B) *anti*-$B_{18}H_{22}$ isomers (green: boron atoms) [A11].

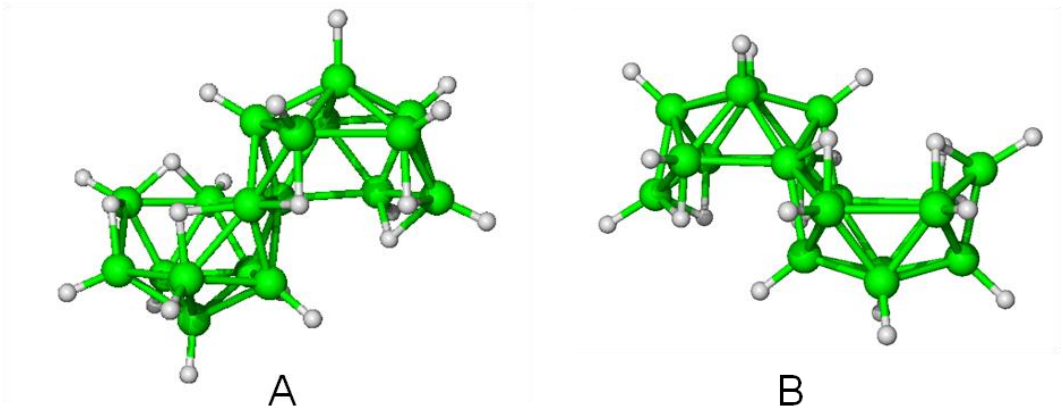

The photophysics of *anti*-$B_{18}H_{22}$ and *syn*-$B_{18}H_{22}$ were studied by spectroscopic techniques and computational methods [A11]. In air-saturated hexane, *anti*-$B_{18}H_{22}$ showed fluorescence with a high quantum yield and some $O_2(^1\Delta_g)$ production (Table 4). Conversely, the isomer *syn*-$B_{18}H_{22}$ showed no measurable fluorescence, displaying instead much faster, picosecond non-radiative decay of excited singlet states. The computed potential energy hypersurfaces (PEH) for both isomers explained these data, pointing to a deep S_1 minimum for *anti*-$B_{18}H_{22}$ and a conical intersection between its S_0 and S_1 states that lies 0.51 eV higher in energy. Such an energy barrier to non-radiative relaxation is not present in the PEH of *syn*-$B_{18}H_{22}$. The computational analysis of the geometries showed that the determining factor for the dissimilar photophysics of *anti*-$B_{18}H_{22}$ and *syn*-$B_{18}H_{22}$ might be due to significant differences in the geometrical rearrangements at their respective conical intersections.

We also demonstrated that the modification of the fluorescent *anti*-$B_{18}H_{22}$ cluster by thiol groups facilitated intersystem crossing from excited singlet states to a triplet manifold (Table 4) [A12]. In contrast to *anti*-$B_{18}H_{22}$, the energy difference between the S_1 and T_1 states in 4,4'-$(HS)_2$-*anti*-$B_{18}H_{20}$ became relatively small, 0.14 eV. Therefore, the $S_1 \rightarrow T_1$ intersystem crossing was efficient. This enhanced the subsequent $O_2(^1\Delta_g)$ production from a Φ_Δ value of approximately 0.008 to 0.59. Phosphorescence of 4,4'-$(HS)_2$-*anti*-$B_{18}H_{20}$ and the ability to generate $O_2(^1\Delta_g)$ with the high quantum yield are quite exceptional properties in boron hydride cluster chemistry.

Table 4. Photophysical properties of *syn*-$B_{18}H_{22}$ (*syn*) and *anti*-$B_{18}H_{22}$ (*anti*) in air-saturated hexane and 4,4'-$(HS)_2$-*anti*-$B_{18}H_{20}$ (*anti*SH) in air-saturated cyclohexane: λ_{max} is the absorption band maximum, λ_f is the fluorescence band maximum, Φ_f is the fluorescence quantum yield, τ_f is the lifetime of the excited singlet states, λ_p is the phosphorescence band maximum, Φ_T is the quantum yield of the triplet states, τ_T is the lifetime of the triplet states in oxygen-free solution, Φ_Δ is the quantum yield of $O_2(^1\Delta_g)$ formation.

	Abs. spectra	Excited singlet states			Triplet states			$O_2(^1\Delta_g)$
	λ_{max}/nm	λ_f/nm	Φ_f	τ_f/ns	λ_p/nm	Φ_T	τ_T/μs	Φ_Δ
syn	229, 308	-	~ 0	0.075	-	-	< 2	~0.008
anti	215, 272, 329	407	0.97	11.2	-	<0.03	6±2	~0.008
*anti*SH	316, 381,	536	-[a]	0.94	596	-[a]	14	0.59

[a] Not measured.

Of the two known dioxygen complexes with a unique peroxo-trapezoid structure, only in the $[(PMe_2Ph)_4Pt_2(O_2)(B_{10}H_{10})]$ is dioxygen bound reversibly (Figure 8) [A13].[20,21] Transient absorption spectroscopy revealed that dioxygen is released after irradiation on a picosecond timescale with a quantum yield as high as 0.58. The binding/release steps can be repeated many times; dioxygen is released under continuous irradiation, and the photoproduced bimetallaborane cluster $[(PMe_2Ph)_4Pt_2(B_{10}H_{10})]$ rebinds dioxygen in a dark period to again form the original $[(PMe_2Ph)_4Pt_2(O_2)(B_{10}H_{10})]$. Unexpectedly, we observed the formation of $O_2(^1\Delta_g)$ with a low quantum yield $\Phi_\Delta < 0.01$. In this case, the photosensitized formation of $O_2(^1\Delta_g)$ can be excluded because the complex itself has no photosensitizing properties. A plausible explanation was earlier suggested by Seip and Brauer for oxodiperoxo Mo complexes.[22] Singlet oxygen is generated by an allowed transition from an upper singlet state of a peroxo complex, whereas the competitive intersystem crossing to a photochemically active triplet state yields dioxygen in the ground triplet state. The very low value of Φ_Δ indicates that the $O_2(^1\Delta_g)$ channel is of minor importance. To the best of our knowledge, $[(PMe_2Ph)_4Pt_2(O_2)(B_{10}H_{10})]$ is the only example of a complex with the metal-metal bond that binds dioxygen and releases it upon irradiation. The compound has potential to serve as a light-triggered local and instantaneous source of dioxygen.

Figure 8. Molecular structure of the dioxygen complex $[(PMe_2Ph)_4Pt_2(O_2)(B_{10}H_{10})]$ (red: oxygen, blue: platinum, green: boron, black: phosphorus) [A13].

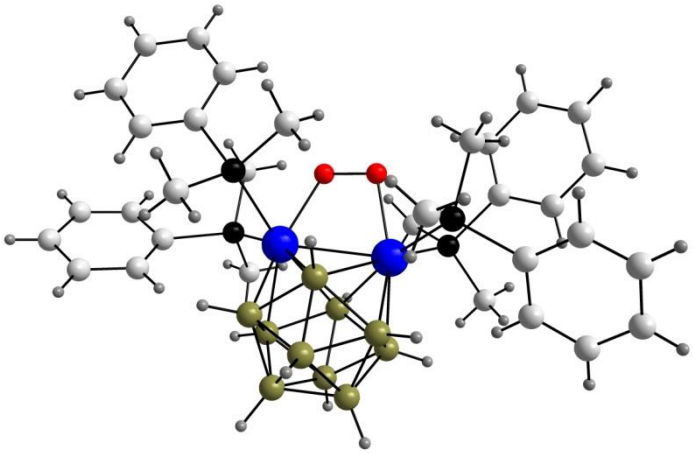

5. Photofunctional materials

The concept of photofunctional materials whose function is triggered by light was introduced by Ogawa and Kuroda.[23] The materials presented in this work were composed of a sensitizer, mostly of the porphyrinic type, and a host (inorganic or organic). The host matrices of well-defined structures can enable the regular organization of the sensitizer molecules and enhance their chemical and photochemical stability. The distribution is especially important in the case of porphyrinic molecules because, due to strong π-π interactions, the porphyrin molecules often form aggregates with reduced or no photochemical activity. Hence, *the hosts can play an active role in controlling the photophysical and photochemical properties of introduced sensitizers.*

The following materials are presented in this thesis:

- *Hybrid layered materials* prepared by intercalation of water-soluble porphyrins into layered double hydroxides (LDHs) [A1,A14-A21] and layered simple hydroxides [A1,A22-A25]. The intercalation provides the arrangement of the guest molecules and eliminates the porphyrin aggregation.
- *Functionalized polymeric nanofibers* with embedded porphyrins and phthalocyanines [A26-A29]. The proper distribution of the embedded molecules, nanometric diameters of the fibers, and proper hydrophilicity of the fiber surfaces were found to be fundamental for the designed photofunction.

The prepared materials can be applied in photosensitized reactions, oxygen sensing, and in the fabrication of bactericidal surfaces.

5.1. Layered hydroxides

The hybrid materials, prepared from layered metal hydroxides, exhibit a compositional variability that makes them promising for a wide range of applications, including catalysis, photovoltaics, polymer nanocomposites, sensing, luminescence, magnetism, and photooxidation. The materials are supposed to be biocompatible carriers that can be used in drug stabilization and delivery systems.

In 1989, Park *et al.* and Dutta *et al.* first described the synthesis and certain properties of the LDH-porphyrin and LDH-phthalocyanine intercalation compounds, respectively.[24,25] Since then, other authors have studied intercalated anionic porphyrins and phthalocyanines, particularly those intercalated into LDHs, and they have contributed to a better understanding of the synthetic methods, structure, and properties imposed by intercalated molecules.[7,26,27] The photophysical and photochemical properties imposed by intercalated porphyrinic compounds have only been studied to a limited extent [A1]. This work summarizes our achievements concerning layered hydroxide hybrids and their synthesis, flexibility, and photofunctionality.

We studied LDHs (Section 5.1.1.), layered zinc hydroxide salts (LZHs) (Section 5.1.2.), and layered rare-earth hydroxides (Section 5.1.3.). Because this work describes many layered hydroxide materials, several notations are used to characterize the composition of the hydroxide layers and the type of intercalated porphyrins. For instance, Mg_RAl-LDH-PdTPPC represents layered double hydroxide with a Mg/Al molar ratio *R* and intercalated with PdTPPC. Analogously, LZH-TPPS is layered zinc hydroxide intercalated with TPPS and LEuH-PdTPPS is layered europium hydroxide intercalated with PdTPPS.

Investigated items:

- Syntheses of layered hydroxide-porphyrin hybrids.
- Structure of layered hydroxide-porphyrin hybrids.
- Absorption and luminescence properties of layered hydroxide-porphyrin hybrids.
- Reactivity of the triplet states of intercalated porphyrins and the formation of $O_2(^1\Delta_g)$.
- Synthesis and properties of composites based on layered hydroxide-porphyrin hybrids.

5.1.1. Layered double hydroxides

The crystal structure of LDHs consists of positively charged metal hydroxide layers and

interlayers composed of anions and water molecules (Figure 9).[28,29] The arrangement of hydroxide layers in LDHs is similar to that of brucite, $Mg(OH)_2$, in which each Mg^{2+} cation is octahedrally surrounded by six OH^- anions and the resulting octahedra share edges to form infinite sheets. The isomorphous substitution of M^{2+} by M^{3+} results in a net positive charge compensated by anionic species in the interlayer space. The chemical composition of LDHs can be represented by the general formula $[M^{2+}_{1-x}M^{3+}_x(OH)_2]^{x+}[A^{n-}_{x/n}]^{x-}\cdot yH_2O$, where M^{2+} and M^{3+} are metal cations in the oxidation states 2+ and 3+, respectively, A^{n-} is an n-valent anion, and *x* usually varies between 0.20 and 0.35.

Figure 9. Structure of LDHs.[30]

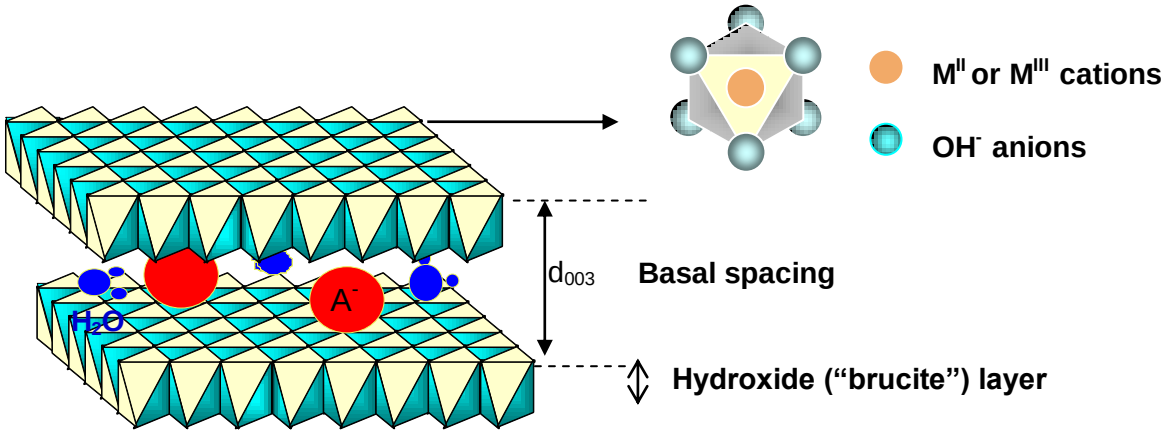

Methods used for the syntheses of LDH-porphyrin hybrids.

- Anion-exchange method. Porphyrins were intercalated by dispersing LDHs, which contained univalent chloride or nitrate anions that have weak electrostatic interactions with the hydroxide layers, in aqueous solutions of anionic porphyrins. The method was not very effective because only a partial exchange occurred and the product contained the LDH precursors.
- Coprecipitation. This was the most effective method for the preparation of pure crystalline LDH-porphyrin hybrids. The method is based on the slow addition of solutions of metal salts (e.g., Al^{3+}, Mg^{2+}; Al^{3+}, Zn^{2+}) mixed in a given molar ratio (*R*) into a reactor containing aqueous solution of the desired interlayer anion. A solution of NaOH is added simultaneously to maintain constant pH. The reaction is performed under a nitrogen atmosphere to eliminate airborne carbon dioxide. After aging, the materials were often subjected to a hydrothermal treatment to increase the sample crystallinity.
- Rehydration of mixed oxides. Mixed oxides were obtained by thermal decomposition of an LDH precursor containing volatile interlayer anions, carbonates, and nitrates at 400-

600 °C. Thereafter, mixed oxides were rehydrated in aqueous porphyrin solution. However, the products were not fully intercalated with porphyrins, and partial metalation of the porphyrin core also occurred.

Arrangement of porphyrins in the LDH interlayer space [A14,A15]. The alignment of intercalated molecules in the galleries of LDHs can be deduced from the analysis of powder XRD patterns. In the case of intercalated porphyrins, the basal spacings d_{003} (Figure 9) varied between 21 and 23 Å, indicating that the size of the interlayer space is comparable to that of the intercalated macrocycle units.

In contrast to other authors, we succeeded in the synthesis of well-crystalline LDH-porphyrin with almost perfect stacking of the hydroxide layers. The high crystallinity of Zn_2Al-LDH-ZnTPPS made it possible to subject the recorded XRD patterns to a full-pattern matching refinement combined with a one-dimensional (1-D) electron density projection [A14] (Figure 10A). The resulting 1-D electron density map displayed two strong maxima at 0 and 23 Å, corresponding to the metal-containing hydroxide layers, and five peaks of lower electron densities between these layers. The five peaks were attributed to the aligned intercalated porphyrin and water molecules. Based of these data, the porphyrin sulfonate groups must be located at a distance of approximately 4 Å from the center of the hydroxide layer. This confirms that hydrogen bonding occurs between the sulfonate groups and the OH groups of the layers. The splitting of the central maximum indicates an orientation disorder of the porphyrin molecules around the central plane.

Figure 10. Zn_2Al-LDH-ZnTPPS: (A) Profile analysis of the XRD pattern recorded in the Debye-Scherrer geometry: experimental X-ray diffraction (circles), calculated (line), Bragg reflections (ticks), and difference profiles. (B) High-resolution TEM micrograph. [A14]

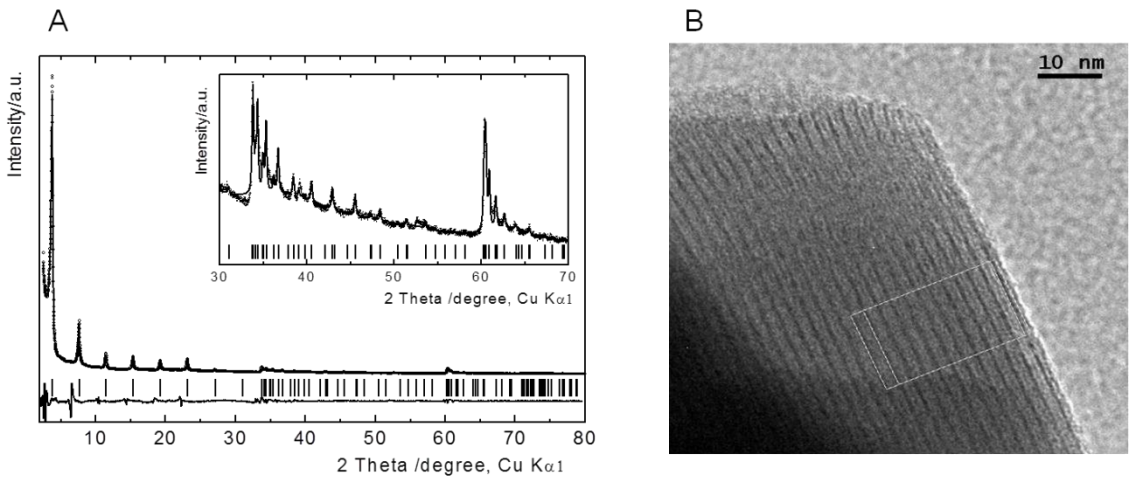

The arrangement of ZnTPPS in Zn_2Al-LDH-ZnTPPS was also studied by high-resolution transmission electron microscopy (HRTEM). The distance between the observed parallel fringes was in good agreement with the d_{003} value of 23.03 Å determined by powder XRD (Figure 10B). The HRTEM micrographs revealed additional lattice fringes with a fringe separation of approximately 8 Å. This separation indicates an increase of electron density in the middle of the interlayer space and confirms the alignment of Zn ions of the ZnTPPS units in the central plane.

The experimental results were complemented by molecular simulations (Figure 11). In agreement with the XRD analysis, the modeled arrangement of ZnTPPS in the Zn_2Al-LDH interlayer space confirmed the disorder of the porphyrin molecules. The interlayer space is filled with nearly parallel porphyrin units, inclined with an average angle of 14° with respect to the hydroxide layers (see also Table 5). Porphyrin zinc atoms are located in the middle of the interlayer space. In comparison, the TPPS units in Mg_2Al-LDH-TPPS are more inclined, and the absence of the central metal in TPPS causes deviations of the porphyrin units from the planarity [A15]. Our results contribute significantly to the description of the two-dimensional arrangement of the porphyrin molecules in the interlayer space of LDHs.

Figure 11. Side view of the interlayer space: (A) Zn_2Al-LDH lattice filled with ZnTPPS [A14]. (B) Mg_2Al-LDH lattice filled with TPPS [A15].

(A) (B)

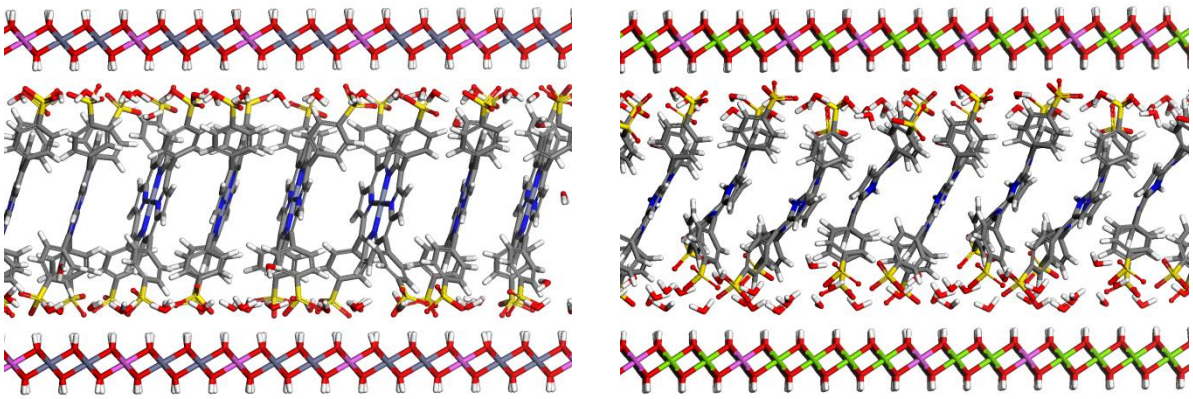

Absorption spectra of intercalated porphyrins. UV/Vis absorption spectra of porphyrins are sensitive to macrocycle-macrocycle interactions, including the formation of aggregates. Typical spectral features can be illustrated on transparent Mg_2Al-LDH-DS films intercalated with TPPS and PdTPPS [A16] since the porphyrin spectra minimally interfere with absorption and light scattering of the LDH host itself. In comparison with the sharp Soret band of monomeric TPPS, its intercalation caused broadening of the Soret band with a maximum at

416 nm, a more noticeable shoulder at approximately 405 nm, and a red shift of Q-bands (Figure 12A). The Soret band of PdTPPS in Mg_2Al-LDH-DS/PdPPS films was also broadened and the Q(1,0) band was red-shifted by 3 nm in comparison with monomeric PdTPPS. The absorption spectra of these films were similar to those recorded for Mg_2Al-LDH-PdTPPC [A17], Zn_RAl-LDH-ZnTPPS and Mg_RAl-LDH-TPPS (R = 2 or 4) [A14,A17,A18], and Zn_RAl-LDH-PdTPPC (R = 2 or 4) [A19] powders. The absence of close contacts of the porphyrin units was confirmed also for Zn_4Al-LDH-PdTPPC by extended X-ray absorption fine structure measurement (EXAFS) [A19]. The observed fact that extensive porphyrin π-π stacking does not take place within the LDH interlayer space was an important prerequisite for the fabrication of photoactive polymer composites [A19,A20,A21].

Figure 12. (A) UV/Vis absorption spectra of the Mg_2Al-LDH-DS/TPPS films deposited on a quartz slide after treatment with aqueous 10^{-4} M TPPS for 5 (b), 15 (c), 30 (d), and 180 min (e) at 50 °C, compared with the original Mg_2Al-LDH-DS film (a) and aqueous solution of TPPS (f). (B) Corresponding normalized fluorescence emission. [A16]

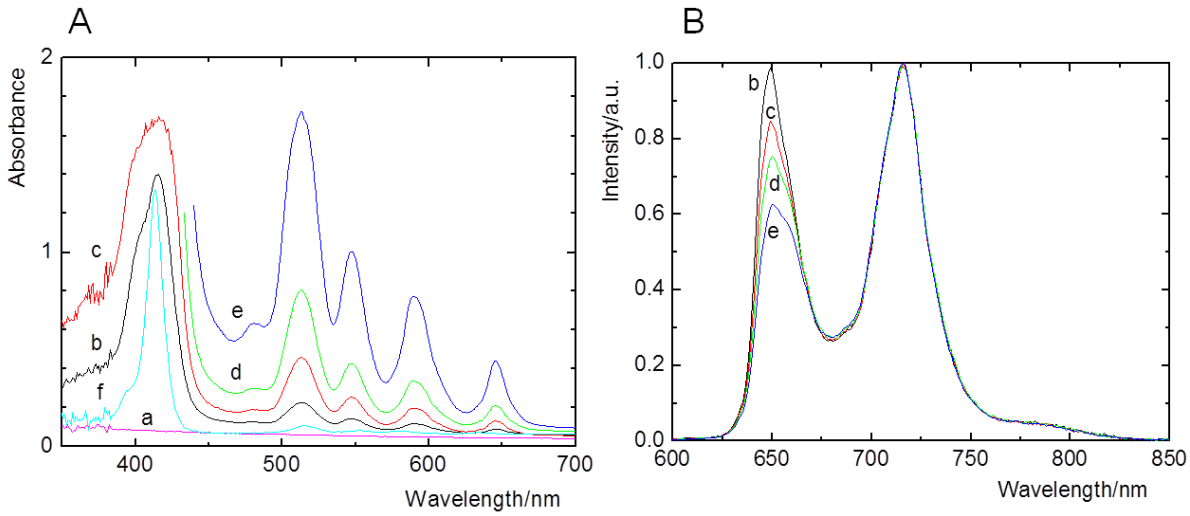

Excited singlet states of intercalated porphyrins. The Q(0,0) and Q(0,1) fluorescence bands of intercalated TPPS in Mg_2Al-LDH-DS films were slightly shifted to 649 and 716 nm, respectively, in comparison with the corresponding bands of monomeric TPPS in aqueous solution at 642 and 703 nm [A16] (Figure 12B). In addition, the intensity of the Q(0,1) band increased at the expense of the Q(0,0) band, and the two fluorescence lifetimes that characterize the fluorescence decay curves were shortened as the loading of TPPS in the LDH film increased. These results show that the porphyrin molecules located in the interlayer space of the LDH host remain photoactive. The observed fluorescence changes were attributed to different porphyrin microenvironments (hydrogen bonding, packing of the TPPS units, *etc*.).

We showed that TPPS intercalated in Mg_2Al-LDH-DS films emits singlet oxygen-sensitized delayed fluorescence (SODF) [A16], similar to TPP embedded in polymeric nanofibers [A26] (Section 5.2.). The repopulation of excited singlet states, $^1P^*$, proceeds *via* the reaction of triplet states, ^3P, with $O_2(^1\Delta_g)$ (Eq. 8) in solids with high concentration of the immobilized ^3P, high local concentration of generated $O_2(^1\Delta_g)$, and adequate oxygen mobility. The analysis of SODF decay curves allowed for estimation of the $O_2(^1\Delta_g)$ lifetime in the LDH interlayer space (see below).

$$^3P + O_2(^1\Delta_g) \rightarrow {}^1P^* + O_2(^3\Sigma_g^-) \qquad (8)$$

Triplet states of intercalated porphyrins. The effects of the hydroxide layers on the triplet state dynamics predetermine the efficacy of the sensitized $O_2(^1\Delta_g)$ generation (Eq. 4). The triplet states of intercalated TPPS in Mg_2Al-LDH-DS films decayed with a lifetime of approximately 500 μs in the absence of oxygen, which is comparable to the lifetime of TPPS in solution. The result indicates that the hydroxide layers do not quench the triplet states in a measurable way [A16,A18]. The decay was accelerated by oxygen but to a lesser extent than in a solvent, due to slower oxygen diffusion in the solid LDH matrix. Because PdTPPS is phosphorescent, the triplet states of intercalated PdTPPS in Mg_2Al-LDH-DS films were probed by luminescence spectroscopy [A16]. These measurements showed that the triplet state quenching by oxygen did not follow first-order kinetics. This observation was interpreted by a broad distribution of the triplet lifetimes. The kinetic heterogeneity of the PdTPPS triplet states was much larger than that of intercalated TPPS.

The porphyrin triplet states in Mg_2Al-LDH-PdTPPC and Mg_2Al-LDH-TPPS powders were probed by transient diffuse reflectance spectroscopy [A17]. Difference absorption spectra showed typical features of the porphyrin triplet states, *i.e.*, a broad positive absorption band in the ~400-550 nm region arising from the triplet-triplet absorption, which is partially depleted by the ground state absorption associated with the Soret band (~400-420 nm) and Q-bands (~500-520 nm). In the absence of oxygen, the observed decay curves were fitted by biexponential functions. It can indicate different locations of intercalated porphyrins and/or conformational deformations of the porphyrin ring yielding distinctly different triplet states. Comparison of the triplet state lifetimes of powder samples (7.1 and 68 μs for Mg_2Al-LDH-TPPS, 3.1 and 50 μs for Mg_2Al-LDH-PdTPPC) with those of free porphyrins in solution indicate deactivation of the triplet states by the LDH host. This is a different behavior than that described above for the LDH films. Probably, remaining intercalated dodecyl sulfate anions used for the pre-expansion of the LDH interlayer space minimizes quenching effects of

the hydroxide layers. The triplet state decay was accelerated by oxygen also in the powder samples, confirming that the sensitizer molecules were accessible to oxygen. The fact that the decay curves in air were fairly fitted with a biexponential function corroborated that the pertinent porphyrin triplet states have different oxygen accessibility.

Time-resolved spectroscopic techniques were also applied to assess the triplet state behavior of the porphyrin sensitizers in LDH/polymer composites [A19]. For example, the triplet state lifetimes of TPPS in polyurethane composites decreased from 1.4–3.0 ms in vacuum to 60–100 μs in oxygen atmosphere. These relatively long lifetimes confirm the limited diffusion of oxygen in the composites.

Singlet oxygen produced by intercalated porphyrins. Typical results confirming the production of $O_2(^1\Delta_g)$ by intercalated TPPS in Mg_2Al-LDH-DS films are presented in Figure 13A [A16]. The luminescence curves recorded at 1270 nm decreased monoexponentially, giving apparent $O_2(^1\Delta_g)$ lifetimes of 7 and approximately 20 μs in oxygen and in air, respectively. The corresponding luminescence band of $O_2(^1\Delta_g)$ is shown in the inset. The fact that the lifetimes were affected by oxygen pressure and that the triplet lifetimes of TPPS obtained by transient absorption spectroscopy had comparable values implies that the rate-determining step of $O_2(^1\Delta_g)$ formation is the decay of the parental TPPS triplet states (see Eq. 4) [A16, A18]. The intrinsic lifetime of $O_2(^1\Delta_g)$ was estimated by kinetic analysis of the SODF curves - the lifetime was approximately 0.3 μs, which is much shorter than the lifetime of $O_2(^1\Delta_g)$ in water ($\tau_\Delta \sim 3.5$ μs). This result points to the vibrational quenching of $O_2(^1\Delta_g)$ by the OH groups coordinated to the metal centers of the hydroxide layers and by water molecules confined in the interlayer space. The short lifetime of $O_2(^1\Delta_g)$ accounts for the low probability of $O_2(^1\Delta_g)$ reactions with molecules surrounding the LDH host.

LDH powders intercalated with TPPS, PdTPPS, or PdTPPC sensitizers also produced $O_2(^1\Delta_g)$ [A17]. This ability was not affected by sample crystallinity. Mg_2Al-LDH-PdTPPC powders in particular were found to be good producers of $O_2(^1\Delta_g)$ [A17]. The $O_2(^1\Delta_g)$ lifetimes recovered from the fitting of the time-resolved luminescence were 10-50 μs longer than those of their precursor triplet states. This indicates that the $O_2(^1\Delta_g)$ molecules generated in the interior of the LDHs have enough time to diffuse out of the LDH host. It was proven in the suspensions of Mg_2Al-LDH-PdTPPC, in which the lifetimes of produced $O_2(^1\Delta_g)$ were governed by the solvent itself.

Intercalated ZnTPPS and ZnTPPC behaved differently [A14, see also for LZH-ZnTPPS in A22]. Although zinc porphyrins are effective sensitizers in solution, when intercalated into

LDHs, no detectable luminescence of $O_2(^1\Delta_g)$ was observed. We infer that $O_2(^1\Delta_g)$, if produced, disappears very quickly, within several microseconds after its formation. Consequently, ZnTPPS and ZnTPPC are not suitable sensitizers for the preparation of photofunctional layered hydroxides.

Figure 13. (A) Luminescence signals of $O_2(^1\Delta_g)$ in air (black line) and in an oxygen atmosphere (blue line) after the excitation of TPPS in the Mg_2Al-LDH-DS/TPPS film. The red lines are least squares monoexponential fits. Inset: Emission band of $O_2(^1\Delta_g)$ in air. [A16] (B) Time dependence of the $^1O_2$ luminescence signal at 1270 nm of the Mg_2Al-LDH-PdTPPC sample in O_2 when fresh (a), dehydrated (b), rehydrated by exposure to ambient air (c, red line), and dehydrated again (d, red line) (λ_{exc}= 425 nm, ~1 mJ/pulse). [A17]

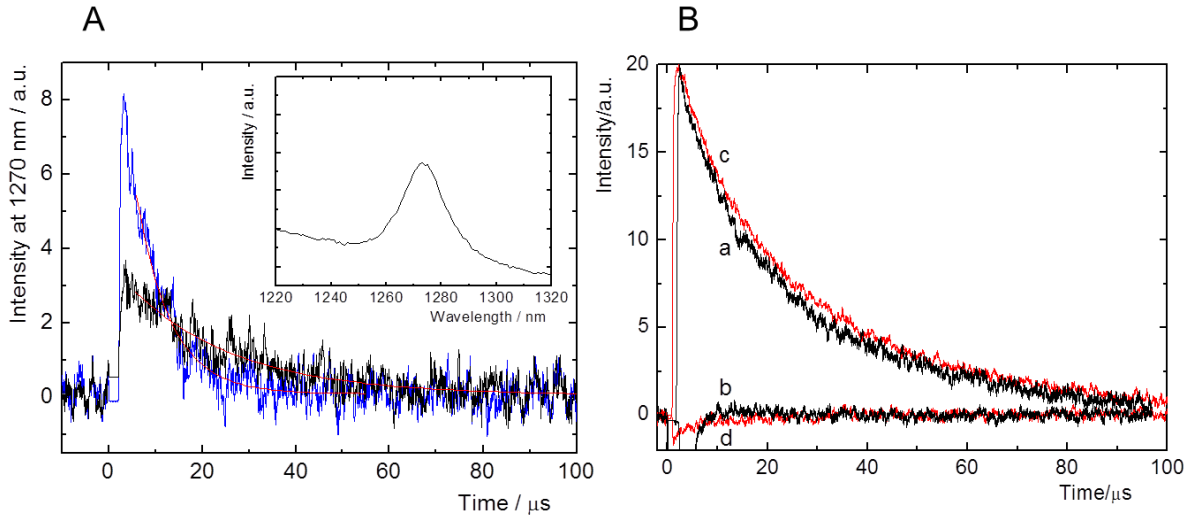

As has been mentioned, the potential application of sensitizer-doped solids as $O_2(^1\Delta_g)$ sources depends not only on the $O_2(^1\Delta_g)$ yield but also on its lifetime. As shown above, the LDH host may influence the lifetime of the photoproduced $O_2(^1\Delta_g)$. Consequently, structural and composition changes of the host may significantly influence the oxidative efficacy of the material. To pursue this issue, we investigated in detail the formation of $O_2(^1\Delta_g)$ sensitized by PdTPPC in dried Mg_2Al-LDH-PdTPPC (Figure 13B) [A17]. Because water is an efficient quencher of $O_2(^1\Delta_g)$, longer $O_2(^1\Delta_g)$ lifetimes were expected for the dehydrated samples. Surprisingly, we observed the opposite behavior; the removal of the interlayer water inhibited the production of $O_2(^1\Delta_g)$. Because the population of the porphyrin triplet states and their relaxation kinetics were not significantly affected by dehydration, the only explanation was that the removal of interlayer water dramatically increases the vibrational quenching of $O_2(^1\Delta_g)$ by the hydroxyl LDH groups. The capability of the dehydrated LDHs to

photogenerate long-lived $O_2(^1\Delta_g)$ was recovered after the exposure of the dried samples to atmospheric humidity. This finding presents Mg_2Al-LDH-PdTPPC as a source of $O_2(^1\Delta_g)$ whose oxidative activity can be modulated by the dehydration/rehydration cycles.

Composite materials. The ability of intercalated porphyrins to produce $O_2(^1\Delta_g)$ upon irradiation with visible light and the known cytotoxicity of $O_2(^1\Delta_g)$ led to the idea to utilize the nanocontainer and nanofiller aspects of LDHs for the preparation of LDH-porphyrin/polymer composites for bactericidal coatings [A19,A20,A21]. We investigated Zn_RAl-LDH and Mg_RAl-LDH functions in polyurethane (PU), poly(butylene succinate), or poly(butyl methacrylate) composites.

PdTPPC and TPPS were intercalated into the LDH hosts by the coprecipitation procedure and then used as fillers in two eco-friendly polymers, namely PU and poly(butylene succinate) [A19]. LDH-porphyrin/polymer composites were prepared either by a solvent cast/cross-linking technique or by melt-compounding with different porphyrin-LDH filler loadings (up to 1.3 wt.%). Both X-ray diffraction and transmission electron microscopy measurements indicated that the porphyrin-LDH fillers are well dispersed in the polymer matrices and that the porphyrin molecules remain intercalated within the LDH hydroxide layers (Figure 14A).

Figure 14. (A) TEM/bright field micrograph of the Zn_3Al-LDH-PdTPPC/PU composite. (B) Decay of the PdTPPC triplet states in the Zn_2Al-LDH-PdTPPC/PU composite film in vacuum (red) and in an oxygen atmosphere (black) recorded at 480 nm. [A19]

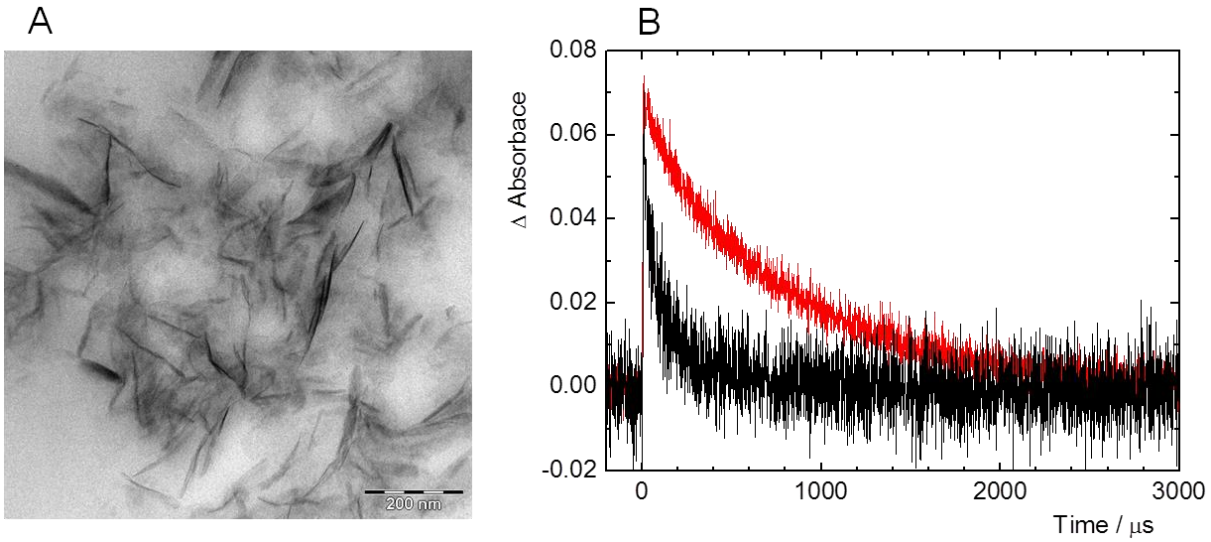

LDHs intercalated with anions containing reactive vinyl groups, namely acrylate, methacrylate, 2-acrylamido-2-methyl-1-propanesulfonate, and 4-vinylbenzoate,

polymerization initiator - 4,4'-azobis(4-cyanopentanoate), and hydrophobic DS, were prepared by anion exchange reactions, in which Mg_2Al-LDH-NO_3 and Zn_2Al-LDH-NO_3 were used as precursors [A20]. These hybrid LDHs were used as co-monomers or initiators for the preparation of LDH/poly(butyl methacrylate) nanocomposites; the preparations were performed by *in situ* emulsion polymerization and solution polymerization in 1-methyl-2-pyrolidone or in a mixture of dimethylformamide and formamide. We obtained nanostructured hybrid materials containing a low amount of the inorganic filler (1 – 5 wt.%); the best dispersion of LDH nanoparticles was obtained in the products prepared by solution polymerization in a mixture of dimethylformamide and formamide (50/50 v/v). Furthermore, LDHs co-intercalated with monomers (methacrylate or 2-acrylamido-2-methyl-1-propanesulfonate) and hydrophobic dodecyl sulfate anions were prepared; at least a low amount of monomer anions had to be intercalated to achieve LDH delamination in the composites. The addition of LDHs decreased the gas permeability of the nanocomposite membranes, but the mechanical properties were not affected. The LDH/poly(butyl methacrylate) nanocomposites producing $O_2(^1\Delta_g)$ were obtained by the partial intercalation of TPPS in LDHs.

Bactericidal properties. The composites were suggested as platforms for the fabrication of bactericidal surfaces activated by visible light. Because the polymer matrix restricts the diffusion of oxygen and partially quenches $O_2(^1\Delta_g)$, the cytotoxic effect on the composite surface is due to $O_2(^1\Delta_g)$ produced in a narrow surface layer. It is promising that the surface concentration of $O_2(^1\Delta_g)$ can be tuned by the amount of intercalated sensitizers and/or by the amount of fillers.

The photostability and photobactericidal properties of Zn_2Al-LDH-PdTPPC/PU composite films were studied to establish their applicability as new photodynamic surfaces [A21]. These films comprised PdTPPC intercalated in Zn_2Al-LDH and dispersed into the PU matrix (1 wt.%). We showed that the Zn_2Al-LDH host enhanced the chemical stability of PdTPPC by minimizing photobleaching and aggregation effects. Investigation of the kinetics of the quenching of the triplet states by oxygen indicated slow diffusion of oxygen within the composite (Figure 14B). The effects of $O_2(^1\Delta_g)$ on the stability of the PU matrix were examined by measuring oxygen consumption and carbon dioxide production under accelerated aging conditions. Oxygen uptake experiments coupled with attenuated total reflectance-FTIR spectroscopy indicated the probable formation of hydroxylated photoproducts, but there were no detrimental effects on the microstructure and viscoelastic

properties of the PU composite.

In vitro antimicrobial tests showed that *Staphylococcus aureus* growth on the composite surfaces is inhibited by white light irradiation. We also observed total inhibition of *Pseudomonas aeruginosa* growth, which indicates the efficacy of the surface against biofilm formation.

To summarize, the activity of the surfaces can be tuned by adjusting the amount of filler. The potential applications of such *photodynamic surfaces, which are sterile under white light,* are of great interest in all cases in which it is desirable to maintain microbial populations at a low level.

5.1.2. Layered zinc hydroxide salts

In contrast to LDHs, layered simple hydroxides consist of hydroxide layers containing a single type of metal cation, with a positive charge created by hydroxyl vacancies. The representatives of this group are $M_2(OH)_3(A^{n-})_{1/n}$ (M = Co, Cu, Ni) and layered zinc hydroxide salts $Zn_5(OH)_8(A^{n-})_{2/n}$ (LZH).[31,32] In the structure of LZHs, a quarter of the octahedrally coordinated zinc ions is replaced by tetrahedrally coordinated zinc ions below and above the plane, thus forming a triple-deck architecture. The attractive aspects of LZHs are their simple synthesis, a high anion-exchange capacity (3.2 meq g^{-1} for LZH-NO_3) that is comparable to LDHs, the possibility of mixing Zn ions with other metal ions (Ni^{2+}, Co^{2+}), and simple transformation to a wide band gap semiconductor, ZnO.

Synthesis of LZH-porphyrin hybrids. LZH-porphyrin hybrids were prepared by precipitation because ion exchange of nitrate anions in $[Zn_5(OH)_8(NO_3)_2]\cdot 2H_2O$ (abbreviated hereafter as LZH-NO_3) for porphyrins led to the formation of ZnO [A22].

During the investigation of intercalation reactions, we discovered that LZHs can delaminate into individual hydroxide layers [A23]. This process provided positively charged hydroxide nanosheets that restack to form hydroxide films of the original LZH structure. The most promising results were obtained with LZHs intercalated with dodecyl sulfate anions (LZH-DS) and LZH-NO_3 delaminated in butanol at 60 °C and delaminated in formamide at room temperature, respectively. The former method produced hydroxide nanosheets with a lateral size of approximately 20 nm. The latter method yielded nanosheets with a size decreasing from approximately 70 nm to 10 nm after two weeks of aging; the thickness of these nanosheets remained nearly constant (3-4 nm). The solvothermal transformation of the hydroxide nanosheets produced nanosheets of ZnO with a thickness of 0.6 - 0.7 nm, corresponding to two or three stacked ZnO tetrahedra layers [A24]. The lateral size varied

between 15 and 25 nm. The ZnO nanosheets were arranged into transparent films with a large {001} surface area by dip-coating and inkjet printing.[33] Such orientation of the high-energy facets {001} allowed for the preparation of transparent, ultrathin ZnO films with superior photocatalytic degradation activity toward 4-chlorophenol.

Arrangement of porphyrins in the LZH interlayer space [A22]. The properties and the arrangement of the porphyrin molecules in the interlayer space were explored by a combination of experimental techniques and molecular simulations. The XRD patterns of LZH-ZnTPPS confirmed the identity of the hydroxide layers and revealed the layered structure with an interlayer space comparable in size to that of ZnTPPS. Molecular simulations of LZH-ZnTPPS showed that the interlayer space is filled with the porphyrin guests: (i) porphyrin planes are inclined with respect to the hydroxide layer normal by approximately 22°; (ii) the angle between the porphyrin planes varies between 0 (parallel arrangement) and 20°; (iii) porphyrin units are tightly arranged; (iv) hydrogen bond interactions between the porphyrin sulfonate groups and the layer OH groups are similar to those observed in LDHs (Section 5.1.1.). The arrangement of ZnTPPS in LZH and Zn_2Al LDH hosts is summarized in Table 5.

Table 5. Comparison of the ZnTPPS arrangement in LZH-ZnTPPS and Zn_2Al-LDH-ZnTPPS hybrids obtained by molecular modeling.

System	Basal spacing	Tilted angle[a]	Angle between planes[b]	Distance between planes[c]
Zn_2Al-LDH-ZnTPPS[A14]	23.0 Å	14°	0 - 10°	5.5 Å
LZH-ZnTPPS[A22]	22.8 Å	22°	0 - 20°	4 Å

[a] Average angle between the layer normal and the porphyrin plane; [b] Angle between the neighboring porphyrin planes varies between 0 (parallel arrangement) and the given maximal value; [c] Average distance between the neighboring porphyrin planes.

Spectral and photochemical properties of intercalated porphyrins [A22]. The absorption spectra of the hybrids confirmed the identity of the intercalated porphyrins. LZH-ZnTPPS behaved similarly to LDH-ZnTPPS, indicating that ZnTPPS loses its photosensitizing activity in general when located between the hydroxide layers. In contrast, both LZH-PdTPPS and LZH-PdTPPC showed intense luminescence signals of photoproduced $O_2(^1\Delta_g)$. The effective $O_2(^1\Delta_g)$ lifetimes were 30 and 41 μs for LZH-PdTPPS and LZH-PdTPPC in an oxygen atmosphere, respectively. Both hybrids appear to be good $O_2(^1\Delta_g)$ producers, indicating that the LZH host is a suitable carrier for Pd porphyrins.

5.1.3. Layered rare-earth hydroxides

Recently, a series of layered rare-earth hydroxides (LREHs) with the general composition $Ln_2(OH)_5(A^-)\cdot xH_2O$ and $Ln_2(OH)_4(A^-)_2\cdot 1.5H_2O$ has been synthesized in the context of increasing interest in their unique ability to combine the properties of lanthanide ions with the host–guest chemistry of layered hydroxides.[34,35]

Tetrasulfonated porphyrins and europium or terbium cations were used to prepare novel hybrid materials whose photophysical properties are controlled by the arrangement of the porphyrin units [A25]. We prepared LREHs with intercalated tetrasulfonated porphyrins corresponding to the formula $Ln_2(OH)_{4.7}(P)_{0.33}\cdot 2H_2O$ (Ln = Eu^{3+}, Tb^{3+}; P = TPPS and PdTPPS). A variation of the synthetic protocol led to a three-dimensional metal-organic framework (as-prepared MOF-Eu-TPPS) made of distorted octahedral oxometalate clusters $[Eu_6(\mu_6\text{-}O)(\mu_3\text{-}OH)_8(H_2O)_{14}]^{8+}$. These secondary building units (SBUs) were linked together by six distorted porphyrin units. During activation, the original SBU lost not only water molecules from the coordination sphere but also the central μ_6-O atom. The loss of the central atom resulted in the distortion of the octahedral $[Eu_6(\mu_6\text{-}O)(\mu_3\text{-}OH)_8(H_2O)_{14}]^{8+}$ SBU into a trigonal antiprismatic $[Eu_6(\mu_3\text{-}OH)_8(H_2O)_2]^{10+}$ SBU with two μ_3-OH groups nearly in plane with the europium ions, and it led to the reduction of pores to approximately 2 × 3 Å. As a result, activated MOF-Eu-TPPS had no accessible porosity. This transformation was thoroughly characterized by single-crystal X-ray crystallographic analysis of both phases.

Photophysical investigations showed that the prepared LREH and MOF materials are fluorescent and have different fluorescence emission spectra (Figure 15A). As shown, LEuH-TPPS produced $O_2(^1\Delta_g)$ after excitation. The observed lifetime of approximately 4 μs in an oxygen atmosphere was very short and demonstrated that the decay of $O_2(^1\Delta_g)$ was controlled by the decay rate of the parental porphyrin triplet states. In the case of LEuH-PdTPPS, no luminescence of $O_2(^1\Delta_g)$ was observed, most likely because the signals were obscured by the scattering of an excitation laser pulse and/or by porphyrin luminescence. Similarly to LDHs, these results corroborate the key effects of hydroxide layers and water molecules confined in the interlayer space on the fate of $O_2(^1\Delta_g)$.

In contrast to LEuH-TPPS, the luminescence of $O_2(^1\Delta_g)$ observed after excitation of solid as-prepared MOF-Eu-TPPS was intensive, making this material the first reported MOF that produces $O_2(^1\Delta_g)$. A relatively long $O_2(^1\Delta_g)$ lifetime of 23 ± 1 μs was observed in both air and oxygen. This result means that the decay of $O_2(^1\Delta_g)$ is much less controlled by the decay of the TPPS triplet states than in the layered structure of LEuH-TPPS. Dehydrated MOF-Eu-

TPPS exhibited a slightly lower $O_2(^1\Delta_g)$ lifetime of 16 ± 1 μs. The shorter lifetime may be related to the more closely packed porphyrin units in this structure (Figure 15B).

The capability of the MOF to produce $O_2(^1\Delta_g)$ stimulates our interest in the design and synthesis of multifunctional porphyrin frameworks with tunable photoresponses and porosity combined with photobactericidal and photooxidation properties.

Figure 15. (A) Normalized fluorescence emission spectra of TPPS in solid LEuH-TPPS (black), LTbH-TPPS (red), as-prepared MOF-Eu-TPPS (green), and dehydrated MOF-Eu-TPPS (blue). Solid samples were excited at 420 nm. (B) Details of the porphyrin unit arrangement in as-prepared MOF-Eu-TPPS obtained by single crystal analysis. [A25]

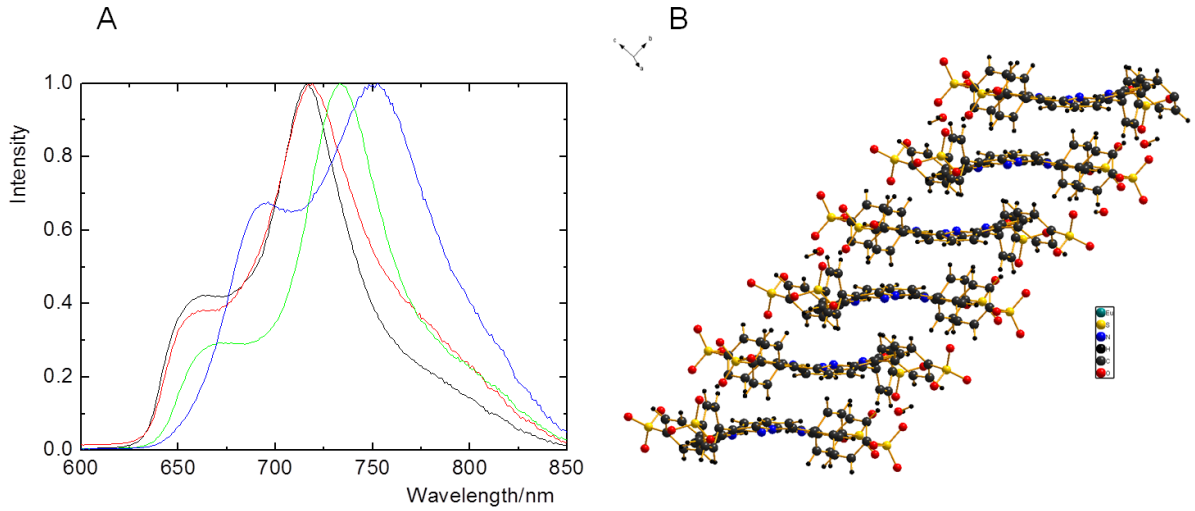

5.2. Polymers

Polymer nanofibers rapidly became widely used as nanostructured materials. Because of their large specific surface, light weight, chemical specificities, low cost, and mechanical flexibility, such nanofibers have already been used in drug delivery, filtration, sensing, engineering, nanoreinforcement, protective clothing, and medicine.

Nanofabrics, composed of functionalized polyurethane (PU) nanofibers (Figure 16), were produced by using an industrial-scale electrospinning method [A26]. A unique photofunction was imparted by embedded TPP, an efficient producer of $O_2(^1\Delta_g)$ in solutions. The absorption and fluorescence emission spectra of embedded TPP were similar to the spectra in CH_2Cl_2. These observations indicated that TPP remains monomeric in PU nanofibers. We also described the preparation and spectral properties of $(nBu_4N)_2[Mo_6I_8(CF_3COO)_6]$ embedded in PU nanofibers [A10] and porphyrin-doped nanofibers made of polystyrene and gelatin,[36] polycaprolactone and polyamide 6 [A29].[37] The diameter of nanofibers is hundreds of nanometers, which is comparable to the oxygen diffusion radius.

Quenching of the triplet states of embedded TPP by oxygen, with a quenching rate constant of 2.5 s^{-1} Pa^{-1}, produced $O_2(^1\Delta_g)$ (Figure 16). The lifetimes of the triplet states were not affected by the surrounding media (Table 6). In contrast, the measured lifetimes of $O_2(^1\Delta_g)$ produced by the nanofabrics placed in D_2O were much shorter than the lifetime of $O_2(^1\Delta_g)$ in pure D_2O (Table 6). The lifetime of $O_2(^1\Delta_g)$ in pure H_2O is approximately 3.5 μs, and it doubles when $O_2(^1\Delta_g)$ is produced by nanofibers immersed in H_2O. The described behavior shows that the produced $O_2(^1\Delta_g)$ was partially quenched by the polymer itself and partially diffused outside the nanofibers into the solvent. Similar results were obtained for embedded ZnTPP and/or zinc phthalocyanine (ZnPc) sensitizers [A27]. The nanofabrics doped by ZnTPP and/or ZnPc efficiently harvested visible light and generated $O_2(^1\Delta_g)$ with a lifetime of approximately 15 μs in air. The energy transfer between the excited singlet states of ZnTPP and the ground states of ZnPc was described in detail. In a series of experiments, we demonstrated that the photoproduced $O_2(^1\Delta_g)$ diffuses from the nanofibers to the surrounding solvent where $O_2(^1\Delta_g)$ can oxidize inorganic or organic compounds [A26,A27].[37]

Figure 16. Scanning electron microscopy of PU nanofibers loaded with TPP (left) and the kinetic traces of the triplet states, $O_2(^1\Delta_g)$, and singlet oxygen-sensitized delayed fluorescence (SODF) (right). [A28]

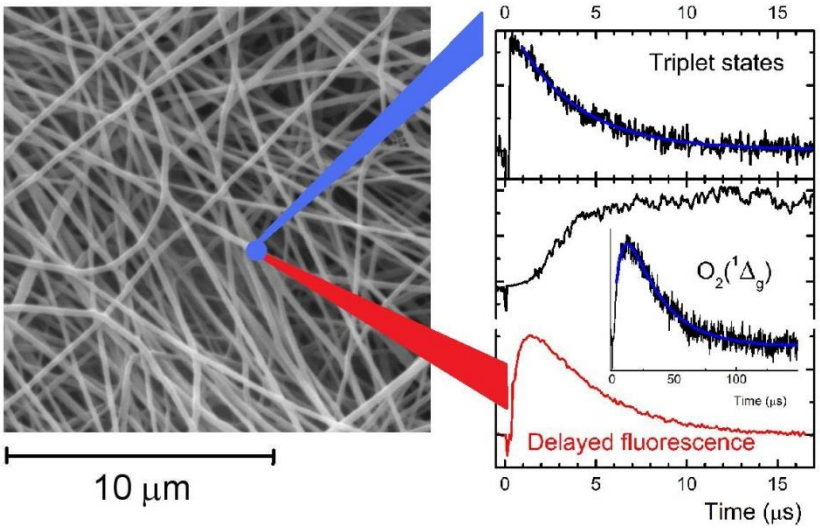

We also observed the emission of SODF by embedded TPP (Figure 16). The dependence of the SODF intensity on excitation laser energy had a quadratic character, indicating that two absorbed quanta are required for the repopulation of the excited singlet states of TPP (Eq. 8). Hence, the emission of SODF requires an oxygen molecule and two porphyrin triplets, one of which is consumed to form $O_2(^1\Delta_g)$ (Eq. 4). The kinetics of SODF was studied in detail in two

consecutive communications [A28].[36] Because the intensity and kinetics of SODF are strongly affected by oxygen concentration in the microenvironment, SODF is a sensitive indicator of the oxygen content. We proposed that SODF spectroscopy could be used for spatially resolved imaging of $O_2(^1\Delta_g)$ inside polymeric nanofibers and other materials.

Table 6. Lifetimes of the porphyrin triplet states (τ_T) and corresponding lifetimes of $O_2(^1\Delta_g)$ (τ_Δ) produced by TPP embedded in PU nanofibers in air or immersed in air-saturated solutions [A26].

Surroundings	τ_T/μs	τ_Δ/μs	
		Measured	Literature[a]
Air	18.1	21.2	-[b]
D_2O	18.3	18.6	68
H_2O	18.0	6.3	3.5
H_2O,0.01M NaN_3	17.9, 2.0 [c]	4.7	-

[a] Lifetime of $O_2(^1\Delta_g)$ in the given environment. [b] Radiative lifetime of unperturbed $O_2(^1\Delta_g)$ is 72 min.

[c] Biexponential decay.

Photoproduced $O_2(^1\Delta_g)$ imparted bactericidal [A26,A27][37,38] and virucidal [A29] properties to porphyrin-doped nanofabrics. The bactericidal properties were demonstrated by testing with the DH5α *Escherichia coli* strain. In control experiments that used doped nanofabrics in the dark or nanofabrics without the incorporated sensitizer exposed to light or kept in the dark, the growth of the bacteria was not affected. The strong photovirucidal effects toward non-enveloped polyomaviruses and enveloped baculoviruses were observed on the surfaces of hydrophilic PU and polycaprolactone nanofibers with embedded TPP. In all cases, we observed that hydrophilicity of the nanofiber surfaces was a prerequisite of nanofiber activity. Surprisingly, the nanofibers exhibited post-irradiation bactericidal properties after long periods of irradiation due to the minor generation of H_2O_2.[37]

The nanofibers are excellent hosts of photoactive compounds. Considering the industrial scale of nanofabric production and the fact that bacteria cannot pass through a nanostructured material because they are retained at the surface, the sensitizer-doped nanofabrics are potentially useful as sterile materials.

6. Conclusions

The presented research concentrated on porphyrinic sensitizers whose spectral and photophysical properties are affected by noncovalent interactions within either molecular assemblies or matrices, which can be inorganic or organic. Many of our results concerning the structure and photophysical properties of free and embedded sensitizers, their intercalation, the delamination of layered hydroxides, and the fabrication of polymeric composites and oriented layers were new and were published for the first time by our team. The investigated topics were:

A) *Synthesis, characterization, and structure of the molecular assemblies and hybrid materials.* The sensitizers were studied in solutions, dispersions, and embedded in the solid materials (powders, films, nanofibers).

B) *Properties of the sensitizer molecules*. Elementary photoprocesses occurring after excitation of the sensitizers (free or bound) were investigated and correlated with the nature of the sensitizer environment. The structural aspects, absorption spectra, luminescence, and sensitizing properties of the molecular assemblies and photofunctional materials were summarized in our review papers [A1].[4,20] The organization of the sensitizers in the materials is an important parameter because these molecules tend to form closely stacked aggregates with reduced photochemical activity. Some of the studied sensitizers have excellent brightness (*i.e.*, product of molar absorption coefficient and luminescence quantum yield), high yields of $O_2(^1\Delta_g)$, and emission in the red region, and they can serve as a platform for the development of novel oxygen sensors, singlet oxygen sensitizers, and UV/Red light convertors.

C) *Functions of the materials*. Some of the investigated materials are good solid-state sensitizers that produce $O_2(^1\Delta_g)$, and they have bactericidal, virucidal, and photocatalytic activities. They also exhibit interesting electrochemical properties. Hence, our research may motivate applications of these materials in the area of photoactive surfaces, catalysts, sensors, molecular magnets, and even batteries.

The main results:

- *Effect of container molecules*. The host molecules influence the spectral and photophysical properties of the sensitizers, especially the lifetimes and quenching rate constants of the sensitizer excited states. It is difficult, however, to form a general model of all the effects because numerous, sometimes opposite factors are combined together: *e.g.*, aggregation, restriction of internal movement, protonation, electron transfer, polarity, and preorganization

of a binding site. These studies also stimulated the development of new cluster-type sensitizers in our laboratory.

- *Concept of photofunctional layered metal hydroxides.* The observation that porphyrin π-π stacking does not occur within the interlayer space of layered hydroxides is essential for the concept of photoactive materials. Further positive effects of the hydroxide matrix on intercalated porphyrins are enhanced thermal and chemical stability and reduction of photobleaching. Intercalation affects photophysical and photochemical properties; however, such important features as luminescence and the quenching of the porphyrin triplet states by oxygen remain preserved. The quenching confirms that the porphyrin molecules are accessible to oxygen and can generate $O_2(^1\Delta_g)$. In many cases, singlet oxygen lifetimes were quite short, even shorter than the lifetime of $O_2(^1\Delta_g)$ in water ($\tau_\Delta \sim 3.5$ μs). This points to the quenching of $O_2(^1\Delta_g)$ by the OH groups, which are coordinated to the metal centers of the hydroxide layers, and the water molecules confined in the interlayer space.

- *Description of the two-dimensional arrangement of the porphyrin molecules in the interlayer space* of layered double hydroxides and layered zinc hydroxide salts by experimental and molecular simulation methods.

- *Nanocontainer and nanofiller aspects of LDHs*. The function of the new LDH-porphyrin/polymer composites is based on the ability of intercalated porphyrins to produce $O_2(^1\Delta_g)$ upon irradiation with visible light. The amount of $O_2(^1\Delta_g)$ at the composite surface can be tuned by varying the filler loading and the amount of intercalated porphyrin in the filler. Since $O_2(^1\Delta_g)$ is cytotoxic, these composites provide a platform for the fabrication of bactericidal surfaces functioning under daylight.

- *Bactericidal and virucidal nanofibers*. Considering the industrial scale of the nanofabric production and the fact that bacteria cannot pass through a nanostructured material and are detained on its surface, the porphyrin-doped nanofabrics are prospective materials that would remain sterile while irradiated by visible light.

- *Transformation of layered rare-earth hydroxide to three-dimensional MOFs.* The MOF has framework-dependent fluorescent properties. The ability of the MOF to produce long-lived $O_2(^1\Delta_g)$ motivates the design of novel MOFs with tuned photoresponses and porosity.

- *Delamination of layered metal hydroxides to hydroxide nanosheets and their use for the preparation of functional films with adjustable thicknesses.* The functions of the nanostructured films prepared from the hydroxide/oxide nanosheets are wide-ranging: (i) luminescent ultrathin films, (ii) transparent films constructed from ZnO nanosheets with

enhanced photocatalytic activity due to the nanosheet orientations,[33] and (iii) electrochemically active ultrathin films with reproducible and stable charge-discharge properties in an alkaline electrolyte.[39]

7. Acknowledgments

K. Lang thanks many colleagues who participated in various parts of the presented research and whose names appear in the cited communications.

8. Publications that form the basis of the thesis

[A1] J. Demel, K. Lang: Layered hydroxide-porphyrin hybrid materials: synthesis, structure, and properties. *Eur. J. Inorg. Chem*. (2012) 5154-5164.

[A2] P. Kubát, K. Lang, K. Procházková, P. Anzenbacher, Jr.: Self-aggregates of cationic meso-tetratolylporphyrins in aqueous solutions. *Langmuir* 19 (2003) 422-428.

[A3] V. Král, F. P. Schmidtchen, K. Lang, M. Berger: Anion-controlled assembly of porphyrin-bicyclic guanidine conjugates. *Org. Lett.* 4 (2002) 51-54.

[A4] K. Lang, P. Kubát, P. Lhoták, J. Mosinger, D. M. Wagnerová: Photophysical properties and photoinduced electron transfer within host-guest complexes of 5, 10, 15, 20-tetrakis(4-N-methylpyridyl)porphyrin with water-soluble calixarenes and cyclodextrins. *Photochem. Photobiol*. 74 (2001) 558-565.

[A5] P. Kubát, K. Lang, P. Lhoták, P. Janda, J. Sýkora, P. Matějíček, M. Hof, K. Procházka, Z. Zelinger: Porphyrin/calixarene self-assemblies in aqueous solution. *J. Photochem. Photobiol. A: Chem.* 198 (2008) 18-25.

[A6] P. Kubát, J. Šebera, S. Záliš, J. Langmaier, M. Fuciman, T. Polívka, K. Lang: Charge transfer in porphyrin-calixarene complexes: ultrafast kinetics, cyclic voltammetry, and DFT calculations. *Phys. Chem. Chem. Phys*. 13 (2011) 6916-6923.

[A7] J. Mosinger, M. Deumié, K. Lang, P. Kubát, D. M. Wagnerová: Supramolecular sensitizer: complexation of *meso*-tetrakis(4-sulfonatophenyl)porphyrin with 2-hydroxypropyl-cyclodextrins. *J. Photochem. Photobiol. A: Chem*. 130 (2000) 13-20.

[A8] J. Mosinger, L. Slavětínská, K. Lang, P. Coufal, P. Kubát: Cyclodextrin carriers of positively charged porphyrin sensitizers. *Org. Biomol. Chem.* 7 (2009) 3797-3804.

[A9] K. Kirakci, P. Kubát, J. Langmaier, T. Polívka, M. Fuciman, K. Fejfarová, K. Lang: A comparative study of the redox and excited state properties of $(nBu_4N)_2[Mo_6X_{14}]$ and $(nBu_4N)_2[Mo_6X_8(CF_3COO)_6]$ (X = Cl, Br, or I). *Dalton Trans*. 42 (2013) 7224-7232.

[A10] K. Kirakci, P. Kubát, M. Dušek, K. Fejfarová, V. Šícha, J. Mosinger, K. Lang: Highly luminescent hexanuclear molybdenum cluster: a promising candidate toward photoactive materials. *Eur. J. Inorg. Chem*. (2012) 3107-3111.

[A11] M. G. S. Londesborough, D. Hnyk, J. Bould, L. Serrano-Andrés, V. Sauri, J. M. Oliva, P. Kubát, T. Polívka, K. Lang: Distinct photophysics of the isomers of $B_{18}H_{22}$ explained. *Inorg. Chem*. 51 (2012) 1471−1479.

[A12] V. Saurí, J. M. Oliva, D. Hnyk, J. Bould, J. Braborec, M. Merchán, P. Kubát, I. Císařová, K. Lang, M. G. S. Londesborough: Tuning the photophysical properties of *anti*-$B_{18}H_{22}$: efficient intersystem crossing between excited singlet and triplet states in new 4,4'-$(HS)_2$-*anti*-$B_{18}H_{20}$. *Inorg. Chem*. 52 (2013) 9266-9274.

[A13] J. Bould, T. Baše, M. G. S. Londesborough, L. A. Oro, R. Macías, J. D. Kennedy, P. Kubát, M. Fuciman, T. Polívka, K. Lang: Reversible capture of small molecules on bimetallaborane clusters: synthesis, structural characterization, and photophysical aspects. *Inorg. Chem. 50* (2011) 7511-7523.

[A14] E. Káfuňková, C. Taviot-Guého, P. Bezdička, M. Klementová, P. Kovář, P. Kubát, J. Mosinger, M. Pospíšil, K. Lang: Porphyrins intercalated in Zn/Al and Mg/Al layered double hydroxides: properties and structural arrangement. *Chem. Mater*. 22 (2010) 2481-2490.

[A15] P. Kovář, M. Pospíšil, E. Káfuňková, K. Lang, F. Kovanda: Mg-Al layered double hydroxide intercalated with porphyrin anions: molecular simulations and experiments. *J. Mol. Model.* 16 (2010) 223-233.

[A16] M. Jiřičková, J. Demel, P. Kubát, J. Hostomský, F. Kovanda, K. Lang: Photoactive self-standing films made of layered double hydroxides with arranged porphyrin molecules. *J. Phys. Chem. C* 115(44) (2011) 21700–21706.

[A17] K. Lang, P. Bezdička, J. L. Bourdelande, J. Hernando, I. Jirka, E. Káfuňková, F. Kovanda, P. Kubát, J. Mosinger, D. M. Wagnerová: Layered double hydroxides with intercalated porphyrins as photofunctional materials: subtle structural changes modify singlet oxygen production. *Chem. Mater*. 19 (2007) 3822-3829.

[A18] K. Lang, P. Kubát, J. Mosinger, J. Bujdák, M. Hof, P. Janda, J. Sýkora, N. Iyi: Photoactive Oriented Films of Layered Double Hydroxides. *Phys. Chem. Chem. Phys*. 10 (2008) 4429-4434.

[A19] E. Káfuňková, K. Lang, P. Kubát, M. Klementová, J. Mosinger, M. Šlouf, A.-L. Troutier-Thuilliez, F. Leroux, V. Verney, C. Taviot-Guého: Porphyrin-layered double

hydroxide/polymer composites as novel ecological photoactive surfaces. *J. Mater. Chem*. 20 (2010) 9423-9432.

[A20] F. Kovanda, E. Jindová, K. Lang, P. Kubát, Z. Sedláková: Preparation of layered double hydroxides intercalated with organic anions and their application in LDH/poly(butyl methacrylate) nanocomposites. *Appl. Clay Sci*. 48 (2010) 260-270.

[A21] M. Merchán, T. Sothea Ouk, P. Kubát, K. Lang, C. Coelho, V. Verney, S. Commereuc, F. Leroux, V. Sol, C. Taviot-Guého: Photostability and photobactericidal properties of porphyrin-layered double hydroxide-polyurethane composite films. *J. Mater. Chem. B* 1 (2013) 2139-2146.

[A22] J. Demel, P. Kubát, I. Jirka, P. Kovář, M. Pospíšil, K. Lang: Inorganic-organic hybrid materials: layered zinc hydroxide salts with intercalated porphyrin sensitizers. *J. Phys. Chem. C* 114 (2010) 16321-16328.

[A23] J. Demel, J. Pleštil, P. Bezdička, P. Janda, M. Klementová, K. Lang: Layered zinc hydroxide salts: Delamination, preferred orientation of hydroxide lamellae, and formation of ZnO nanodiscs. *J. Colloid Inter. Sci*. 360 (2011) 532-539.

[A24] J. Demel, J. Pleštil, P. Bezdička, P. Janda, M. Klementová, K. Lang: Few-layer ZnO nanosheets: preparation, properties, and films with exposed {001} facets. *J. Phys. Chem. C* 115 (2011) 24702-24706.

[A25] J. Demel, P. Kubát, F. Millange, J. Marrot, I. Císařová, K. Lang: Lanthanide-porphyrin hybrids: from layered structure to metal-organic frameworks with photophysical properties. *Inorg. Chem*. 52 (2013) 2779-2786.

[A26] J. Mosinger, O. Jirsák, P. Kubát, K. Lang, B. Mosinger: Bactericidal nanofabrics based on photoproduction of singlet oxygen. *J. Mater. Chem*. 17(2) (2007) 164 – 166.

[A27] J. Mosinger, K. Lang, P. Kubát, J. Sýkora, M. Hof, L. Plíštil, B. Mosinger Jr.: Photofunctional polyurethane nanofabrics doped by zinc tetraphenylporphyrin and zinc phthalocyanine photosensitizers. *J. Fluoresc*. 19 (2009) 705–713.

[A28] J. Mosinger, K. Lang, L. Plíštil, S. Jesenská, J. Hostomský, Z. Zelinger, P. Kubát: Fluorescent polyurethane nanofabrics: a source of singlet oxygen and oxygen sensing. *Langmuir* 26 (2010) 10050-10056.

[A29] Y. Lhotáková, L. Plíštil, A. Morávková, P. Kubát, K. Lang, J. Forstová, J. Mosinger: Virucidal nanofiber textiles based on photosensitized production of singlet oxygen. *PLoS ONE* 7(11) (2012) e49226.

9. References

1. J. Zhao, W. Wu, J. Sun, S. Guo, *Chem. Soc. Rev*. 42 (2013) 5323-5351.

2. P. R. Ogilby, *Chem. Soc. Rev*. 39 (2010) 3181-3209.

3. R. Schmidt, *Photochem. Photobiol*. 82 (2006) 1161-1177.

4. K. Lang, J. Mosinger, D. M. Wagnerová, *Coord. Chem. Rev*. 248 (2004) 321-350.

5. C. S. Foote, *Photochem. Photobiol*. 54 (1991) 659.

6. See *e.g*., a) P. Kubát, K. Lang, P. Anzenbacher Jr., K. Jursíková, V. Král, B. Ehrenberg, *J. Chem. Soc., Perkin Trans. 1* (2000) 933-941; b) M. Dudič, P. Lhoták, I. Stibor, K. Lang, P. Prošková, *Org. Lett*. 5 (2003) 149-152; c) P. Kubát, K. Lang, P. Janda, P. Anzenbacher, *Langmuir* 21 (2005) 9714-9720; d) V. Novakova, P. Zimcik, M. Miletin, L. Vachova, K. Kopecky, K. Lang, P. Chábera, T. Polívka, *Phys. Chem. Chem. Phys*. 12 (2010) 2555-2563; e) V. Novakova, L. Lochman, I. Zajícová, K. Kopecky, M. Miletin, K. Lang, K. Kirakci, P. Zimcik, *Chem. Eur. J.* 19 (2013) 5025-5028.

7. S. Bonnet, C. Forano, A. de Roy, J. P. Besse, P. Maillard, M. Momenteau, *Chem. Mater.* 8 (1996) 1962-1968.

8. a) A. Čeklovský, A. Czímerová, K. Lang, J. Bujdák, *J. Luminescence* 129 (2009) 912-918; b) J. Bujdák, J. Jurečeková, H. Bujdáková, K. Lang, F. Šeršen, *Environ. Sci. Technol.* 43 (2009) 6202-6207; c) A. Čeklovský, A. Czímerová, K. Lang, J. Bujdák, *Pure Appl. Chem*. 81 (2009) 1385-1396; d) J. Bujdák, M. Danko, D. Chorvát Jr., A. Czímerová, J. Sýkora, K. Lang, *Applied Clay Sci*. 65–66 (2012) 152–157.

9. E. A. Lissi, M. V. Encinas, E. Lemp, M. A. Rubio, *Chem. Rev*. 93 (1993) 699-723.

10. M. Nishio, M. Hirota, Y. Umezawa, *The CH/π Interaction; Evidence, Nature, and Consequences*. Wiley-VCH Publishers, New York 1998.

11. F. Perret, A. W. Coleman, *Chem. Commun.* 47 (2011) 7303–7319.

12. J. Szejtli, *Chem. Rev*. 98 (1998) 1743-1753.

13. K. A. Connors, *Chem. Rev*. 97 (1997) 1325-1357.

14. J. Mosinger, V. Kliment, Jr., J. Sejbal, P. Kubát, K. Lang, *J. Porphyrins Phthalocyanines* 6 (2002) 514-526.

15. A. W. Maverick, J. S. Najdzionek, D. Mackenzie, D. G. Nocera, H. B. Gray, *J. Am. Chem. Soc*. 105 (1983) 1878-1882.

16. J. A. Jackson, C. Turro, M. D. Newsham, D. G. Nocera, *J. Phys. Chem.* 94 (1990) 4500-4507.

17. a) L. M. Robinson, D. F. Shriver, *J. Coord. Chem.* 37 (1996) 119-129; b) O. A. Adamenko, G. V. Loukova, V. A. Smirnov, *Russ. Chem. Bull.* 51 (2002) 994-997; c) N. Prokopuk, C. S. Weinert, D. P. Siska, C. L. Stern, D. F. Shriver, *Angew. Chem., Int. Ed.* 39 (2000) 3312-3315, d) L. F. Szczepura, K. A. Ketcham, B. A. Ooro, J. A. Edwards, J. N. Templeton, D. L. Cedeno, A. J. Jircitano, *Inorg. Chem.* 47 (2008) 7271-7278.
18. A. R. Pitochelli, M. F. Hawthorne, *J. Am. Chem. Soc.* 84 (1962) 3218.
19. V. V. Volkov, E. A. Il'inchik, O. V. Volkov, O. O. Yuryeva, *Chem. Sustainable Dev.* 8 (2000) 185-191.
20. D. M. Wagnerová, K. Lang, *Coord. Chem. Rev*. 255 (2011) 2904-2911.
21. a) J. Bould, Y. M. McInnes, M. J. Carr, J. D. Kennedy, *Chem. Commun.* (2004) 2380-2381; b) J. Bould, C. A. Kilner, J. D. Kennedy, *Dalton Trans.* (2005) 1574-1582.
22. M. Seip, H.-D. Brauer, *J. Photochem. Photobiol. A: Chem*. 79 (1994) 19-24.
23. M. Ogawa, K. Kuroda, *Chem. Rev*. 95 (1995) 399-438.
24. I. Y. Park, K. Kuroda, C. Kato, *Chem. Lett.* (1989) 2057-2058.
25. P. K. Dutta, M. Puri, *J. Phys. Chem*. 93 (1989) 376-381.
26. L. Ukrainczyk, M. Chibwe, T. J. Pinnavaia, S. A. Boyd, *J. Phys. Chem*. 98 (1994) 2668–2676.
27. D. Yan, S. Qin, L. Chen, J. Lu, J. Ma, M. Wei, D. G. Evans, X. Duan, *Chem. Commun*. 46 (2010) 8654–8656.
28. F. Leroux, C. Taviot-Guého, *J. Mater. Chem.* 15 (2005) 3628-3642.
29. V. Rives, (Ed.), *Layered Double Hydroxides: Present and Future*, Nova Science Publishers, New York 2001, pp. 251-434.
30. E. Káfuňková, *Porphyrin-layered double hydroxide hybrids as novel photofunctional materials*, PhD Thesis, Charles University in Prague, Praha, Czech Republic, 2010.
31. G. G. C. Arizaga, K. G. Satyanarayana, F. Wypych, *Solid State Ionics* 178 (2007) 1143-1162.
32. G. Rogez, C. Massobrio, P. Rabu, M. Drillon, *Chem. Soc. Rev.* 40 (2011) 1031-1058.
33. J. Hynek, V. Kalousek, R. Žouželka, P. Bezdička, P. Dzik, J. Rathouský, J. Demel, K. Lang, *Langmuir* 30 (2014) 380-386.
34. F. Geng, R. Ma, T. Sasaki, *Acc. Chem. Res*. 43 (2010) 1177-1185.
35. L. J. McIntyre, T. J. Prior, A. M. Fogg, *Chem. Mater.* 22 (2010) 2635-2645.
36. J. Mosinger, K. Lang, J. Hostomský, J. Franc, J. Sýkora, M. Hof, P. Kubát, *J. Phys. Chem. B* 114 (2010) 15773–15779.

37. S. Jesenská, L. Plíštil, P. Kubát, K. Lang, L. Brožová, Š. Popelka, L. Szatmáry, J. Mosinger, *J. Biomed. Mater. Res. A* 99A (2011) 676-683.
38. P. Henke, K. Lang, P. Kubát, J. Sýkora, M. Šlouf, J. Mosinger, *ACS Appl. Mater. Interfaces* 5 (2013) 3776-3783.
39. a) B. Schneiderová, J. Demel, J. Pleštil, P. Janda, J. Bohuslav, D. Ihiawakrim, O. Ersen, G. Rogez, K. Lang, *J. Mater. Chem. A* 1 (2013) 11429-11437; b) B. Schneiderová, J. Demel, J. Pleštil, H. Tarábková, J. Bohuslav, K. Lang, *Dalton Trans.* (2014), in press.